STUDYING POLYMER TRANSLOCATION WITH DISSIPATIVE PARTICLE DYNAMICS AND MONTE CARLO SIMULATIONS

By

Taylor Dunn

University of Prince Edward Island

Charlottetown, PE, Canada

A thesis submitted in partial fulfillment of

the requirements for the Honours Programme

in the Department of Physics

This Thesis is Approved

_____ _____

Signature (Supervisor) Date

_____ _____

Signature (Second Reader) Date

This Thesis is Accepted

_____ _____

Signature (Dean of Science) Date

Abstract

Polymer translocation is a fundamental biological process by which a long, chain-like molecule is transported through a nanometre-scale pore. The phenomenon has received considerable experimental and theoretical interest due to various potential technological applications. One such technology is that of nanopore sequencing, a method of determining the order in which nucleotides occur on a strand of DNA as it is pulled through a nanopore. If its current technological limitations can be overcome, this fast and inexpensive DNA sequencing technique could become a routine medical procedure.

Our goal with this project is to contribute to the current understanding of polymer translocation dynamics. To accomplish this, we utilize the dissipative particle dynamics (DPD) and Metropolis Monte Carlo (MC) simulation methods. In particular, we are interested in the role of hydrodynamics (HD) – the complex behaviour of fluids in motion. Consequently, our model employs an explicit solvent in which a bead-spring polymer is immersed. Systems of free polymers, unbiased translocation and biased translocation were simulated. We found that translocation behaviour and polymer chain relaxation in solvent followed theoretical predictions incorporating HD, confirming our model correctly accounts for the interactions.

We also investigated the dynamics of translocation in the limit where the rate of translocation is sufficiently slow such that the polymer maintains a state of conformational quasi-equilibrium. This condition is fundamental to the Fokker-Planck (FP)

formalism of polymer translocation, which we used to make predictions for translocation time distributions. In the case of unbiased translocation governed by sufficiently high pore friction, the FP prediction was found to agree with simulation, but more work needs to be done to precisely identify the quasi-equilibrium regime.

Preliminary simulations of biased polymer translocation between good and poor solvent reservoirs yielded preferential translocation towards the better solvent, as expected. The quasi-equilibrium condition was not met in these simulations, however, but should be attainable through higher driving force (solvent quality asymmetry) and pore friction.

Contents

List of Figures

Chapter 1

Introduction

The purpose of this thesis is to examine the conformational behaviour of polymers in the presence of hydrodynamics, quantify the dynamics of polymer translocation through nanopores, and to evaluate the feasibility of the dissipative particles dynamics simulation method for studying polymer translocation. In this chapter, we review relevant background information and definitions, as well as the overarching motivation for the project.

1.1 Polymers

Polymers are a class of macromolecules consisting of many similar or identical building blocks that form a chain-like structure. These building blocks are smaller molecules called monomers, and are linked together by covalent bonds. While the word polymer is often used synonymously with plastic, the classification goes far beyond that. Cellulose, a natural biopolymer, is the most common organic compound on Earth, and is a major component of the tough walls that enclose plant cells [1]. Another example

of a polymeric compound is the polynucleotide which, as the name suggests, consists of monomers called nucleotides. All living cells contain these polymers in the form of the nucleic acids: deoxyribonucleic acid (DNA) and ribonucleic acid (RNA). Together, DNA and RNA store and transfer the entirety an organism's genetic information [2]. Whether they be of the natural or synthetic variety, the ubiquity and applicability of polymers has generated considerable interest in a growing list of fields such biomedical engineering [3], nanotechnology [4] and electronics [5].

In the study of polymers, we are often concerned with their behaviour in solvent. An important consideration for these systems is that of hydrodynamics (HD), or the dynamics of fluids in motion. As a monomer moves through a dilute solvent, it induces a velocity field in the fluid which will be felt by other particles caught in the flow. Effectively, this amounts to surrounding monomers being dragged along by the monomer in motion [6]. Building on the non-HD work of Rouse [7], these HD interactions became the basis for the Zimm model [8], which has proven to be one of the most successful and influential theories in the history of polymer dynamics. In the attempt to incorporate HD and represent a real system as closely as possible, we use the dissipative particle dynamics method — a computer simulation technique.

1.2 DNA Sequencing

As stated earlier, DNA is a biopolymer that stores the entirety of an organism's genetic information. This information is encoded in the sequence of the nucleotides within the molecule, or more specifically the order of the four nitrogenous bases – adenine, guanine, cytosine, and thymine – on a strand of DNA (see Figure 1.1). The

process of determining this order is called DNA sequencing [2], and the information it provides can be used for tailoring medical treatment to patients and for early detection of hereditary diseases [9].

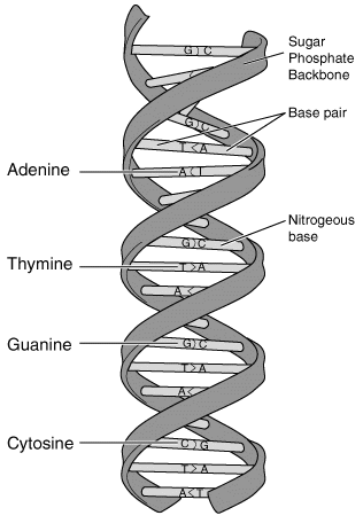

Figure 1.1: The structure and bases of the DNA polynucleotide [10].

Since its inception in 1977, Sanger sequencing has been the most widely-used method of DNA sequencing, owing its success to its relative ease of use and accuracy. To put it simply, the method involves replicating a single strand of DNA, terminating the copies at a specific base (either A, G, C or T), then combining the fragments to get a complete picture [11]. Improvements to Sanger sequencing were a major driving force behind the completion of the Human Genome Project, an international collaborative research project to obtain a complete mapping of the human genome. Despite its importance to this endeavour, Sanger sequencing is an outdated method, costing approximately $10 million, and significant processing time to resequence an individual genome today [12]. At the forefront of DNA sequencing today are various methods that look to resolve base-pair orderings with greater speed and cost efficiency, all while

maintaining the accuracy obtained with Sanger sequencing [13]. One such method, called nanopore sequencing, has the potential to become a fast and inexpensive sequencing technology by making use of the polymer translocation process.

1.3 Polymer Translocation

Polymer translocation involves the transport of a polymer across a membrane through a nanometre-scale pore, and is fundamental to many biological processes. Examples include virus injection, DNA and RNA transport across nuclear pores and protein transport through membrane channels [14, 15]. The pioneering work of Kasianowicz et al. [16] showed the possibility of detecting a translocation event of single-stranded DNA through an α-hemolysin protein channel embedded in a biological membrane. This was done by applying a potential difference across the membrane causing the ions of the solution to traverse the pore, thereby creating a measurable electric current. The negatively charged DNA molecule was also influenced by the potential, pulling it through the nanopore. As the DNA translocated, it blocked the ion flow, causing a measurable drop in current (see Figure 1.2). It was proposed these drops in current are characteristic to the specific nucleotide, so one could identify individual monomers and record their sequence as they passed through the pore. This is the underlying premise for the aforementioned nanopore sequencing technique, and has led to an abundance of experimental work using biological [17–19] and solid-state [20–25] nanopores.

The Achilles' heel of the ultra-fast nanopore sequencing method is just that; the fast rate at which the DNA translocates through the pore makes it difficult to take accurate measurements of the small current fluctuations. In fact, DNA typically translo-

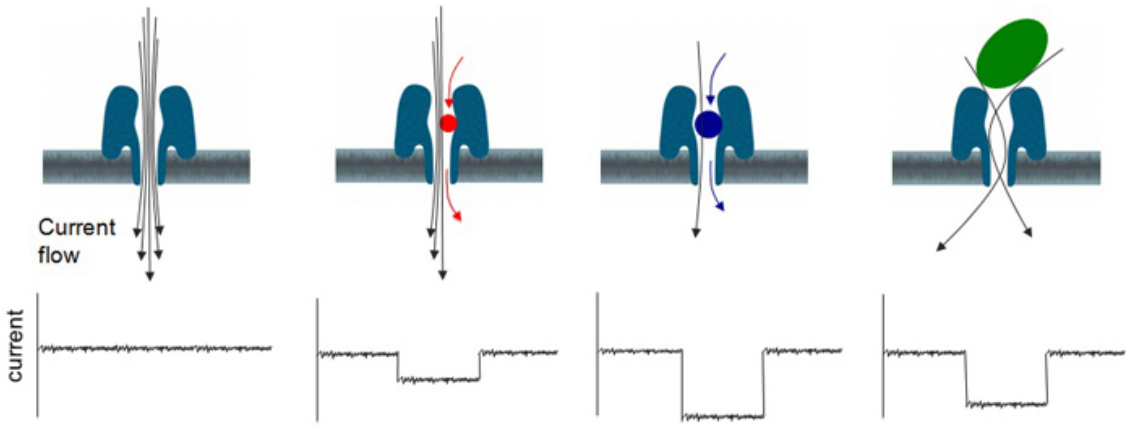

Figure 1.2: A diagram showing how molecules can block ion flow through a nanopore and create characteristic disruptions in the measured current. These measurements can be used to distinguish between the four standard DNA bases [26].

cates through an α-hemolysin pore on the order of microseconds per base pair, while a speed on the order of milliseconds in necessary for good resolution [27]. Thus, a key motivation behind many polymer translocation studies is to find methods of slowing down DNA translocation, but first all the factors affecting the dynamics must be understood. Computational studies such as this one are expected to provide valuable insight regarding the physics of translocation and aid in the development of better nanopore device design [28].

1.4 Computer Simulations

Rapid technological advancements in recent years have made computer simulation techniques and numerical methods very powerful tools for the investigation of polymer properties [6]. The main purpose of computer simulations is to bridge the gap between theory and experiment. They can be used to test the validity of theoretical models, as well as mimic experimental systems and make measurements that may not be

realizable in a typical lab setting. In the context of modelling polymeric systems, the level of detail ranges from atomistic to coarse-grained. On the atomistic level, every atom of the system is explicitly represented as an interaction site. Of course this lends itself to producing the most quantitatively accurate behaviour, but at a cost; computational time for simulations with this level of detail can increase enormously as the system size grows larger [29]. To overcome this limitation, a coarse-grained model can be used to reach greater length and time scales in simulations. This involves clustering groups of atoms into larger interaction sites. As such, effective interactions between sites must be designed in a way such that the global and long-time behaviour is as close as possible to the detailed system. By sacrificing the superfluous details, such as chemical composition of individual monomers, coarse-grained polymer systems can be simulated with a greater degree of computational efficiency [30].

A primary issue that has yet to be resolved in computational studies of polymer translocation is the scaling law behaviour of translocation time with chain length, or $\tau \sim N^{\alpha}$. There is an abundance of research reporting different scaling exponents α, as it appears to be affected by numerous factors such as driving force [31], nanopore friction strength [32], pore length and width [33], solvent quality [34], solvent viscosity [35], temperature [36], finite size effects [37], and simulation technique [38]. Of particular interest is the effect of hydrodynamics on the translocation process. The vast majority of studies neglect these interactions, as the realism afforded by incorporating HD comes at the cost of significantly longer simulation time. Molecular dynamics (MD) simulations employing an explicit solvent have proven to naturally exhibit hydrodynamics from the intramolecular interactions [39, 40] but are computationally

inefficient. To mitigate this issue, various mesoscopic simulation methods employing a coarse-grained solvent model have been investigated. Examples include stochastic rotation dynamics (SRD) [41, 42], the Lattice-Boltzmann method [43, 44], and our technique of choice, dissipative particle dynamics (DPD) [34, 45–49].

1.5 Thesis Outline

The remainder of this thesis is organized as follows. Chapter 2 covers the theory of both free and translocating polymers. The dissipative particle dynamics and Monte Carlo techniques are outlined in Chapter 3, as well the multiple-histogram method for calculating free energy. Chapter 4 describes the molecular model and the simulation details. We present and discuss the results of the simulations in Chapter 5. Finally, in Chapter 6 we summarize the project and suggest future work.

Chapter 2

Background Theory

2.1 Equilibrium Behaviour of Free Polymer Chains

Several factors can cause a polymeric molecule to assume different size, shape and dynamical behaviour, including the nature of the solvent, the number of monomers in the chain and the chemical composition of the polymer. Despite this great potential for variation, there exist universal laws that can describe average polymer conformations. We will first define some common quantities used to describe polymer conformations.

2.1.1 Measures of Polymer Conformational Size

The quantities described in this section can be measured through experiment or calculated theoretically, and can be applied to any polymer conformation. The first and most straightforward quantity is the end-to-end distance R_e. It is related to the displacement between the two ends of a chain, or

$$\vec{R}_e = \vec{r}_N - \vec{r}_1, \tag{2.1}$$

where $\vec{r}_i$ defines the position of monomer i in a chain of N monomers. Thus $\vec{r}_1$ and $\vec{r}_N$ describe the positions of the first and last monomers, respectively. During experiment or simulation, the chain can adopt many different conformations, so time-independent averages are taken to ensure an accurate picture of polymer size is achieved. We thus define the root mean square (rms) end-to-end distance as

$$\bar{R}_e = \sqrt{\langle \vec{R}_e \cdot \vec{R}_e \rangle}, \tag{2.2}$$

where the angular brackets $\langle ... \rangle$ denote the ensemble average over all possible chain conformations. This can also be decomposed into the sum of the spatial components:

$$\bar{R}_e^2 = \bar{R}_x^2 + \bar{R}_y^2 + \bar{R}_z^2. \tag{2.3}$$

Depending on the type of system, one can make predictions for the components based on symmetry. In the case of spherical symmetry, a free polymer in solvent for example, we expect that $\bar{R}_x^2 = \bar{R}_y^2 = \bar{R}_z^2 = \frac{1}{3}\bar{R}_e^2$. For a polymer translocating through a nanopore aligned with the z-axis, we expect cylindrical symmetry so $\bar{R}_x^2 = \bar{R}_y^2 \neq \bar{R}_z^2$.

Another important quantity is the radius of gyration R_g, which is a measure of how widely distributed the monomers are about the polymer's centre of mass. Once again taking conformational averages, the mean square radius of gyration is defined:

$$\bar{R}_g^2 = \frac{1}{N}\sum_{i=1}^{N} \langle (\vec{r}_i - \vec{r}_{\mathrm{cm}})^2 \rangle, \tag{2.4}$$

where

$$\vec{r}_{\text{cm}} = \frac{1}{N}\sum_{i=1}^{N}\vec{r}_i, \tag{2.5}$$

is the position vector of the polymer's centre of mass. The same symmetry arguments can be used as they were for $\bar{R}_e$ to make predictions for the radius of gyration.

2.1.2 Polymer Shape and Solvent Quality

The conformations taken by polymers can generally be grouped into three major categories: globule, coil and rod-like (see Figure 2.1). The distinction here can be understood by considering the pairwise interactions that occur when a polymer is dispersed in a solvent. Those interactions include monomer-monomer, monomer-solvent and solvent-solvent. When monomer-monomer is the preferable (less repulsive) interaction over monomer-solvent, the monomers compact together in a globular structure, whereby the solvent particles are excluded from the globule. In this case, the solvent is considered a poor solvent because it does not allow the polymer to swell. Moreover, a solvent is considered good when the monomer-solvent interaction is preferable, which allows the polymer to adopt a coil-like conformation. On average, this corresponds to a roughly spherical shape with radius R_g [14]. The final major conformation occurs when there is a high degree of bending stiffness in the monomer-monomer bonds, leading to restricted rotational motion and a rod-like shape.

Although not considered in this work, another category called ideal is observed by polymers with no non-bonded interactions between monomers due to cancellation of the repulsive and attractive contributions to the energy. Chains exhibit ideal-like behaviour in solvent conditions (temperature and quality) particular to the polymer

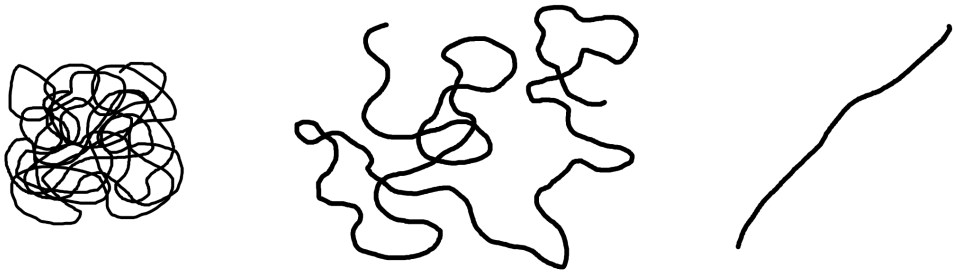

(a) globule (b) coil (c) rod-like

Figure 2.1: The major categories of free polymer conformations.

[6]. In this study, flexible chains in both poor and good solvent are examined, so the shapes of interest are globule and coil. By measuring radius of gyration and end-to-end distance, solvent quality can be determined and polymer shape can be categorized.

2.1.3 Polymer Scaling Relations

In the thermodynamic limit of infinitely long chains, it has been shown that both $\bar{R}_e$ and $\bar{R}_g$ follow a power law with the number of monomers [14]. The proportionality constants are different between the two quantities, and depend on the details of the polymer, but the scaling exponent has no such dependence. Using the generic symbol R to represent the average "size" of the polymer (R_e or R_g), we may write:

$$R \sim N^{\nu}, \tag{2.6}$$

where ν is called the size exponent and depends on solvent quality. For good solvent conditions in which a polymer takes on a coil shape, $\nu \approx 0.588$, and for a globular polymer in poor solvent conditions, $\nu = 1/3$. In the special case of an ideal chain, $\nu = 0.5$, and rod-like chain size scales linearly, so $\nu = 1$ [6]. These discrepancies in

the size exponent tell us that, from largest to smallest overall size, the conformational categories follow the order: rod, coil, ideal and globule.

2.1.4 Relaxation Time and Correlation Functions

An important behaviour in the study of equilibrium polymer dynamics is that of relaxation. The corresponding quantity of interest is the relaxation time τ_r, defined as the characteristic time over which the polymer conformation changes appreciably, and thus becomes uncorrelated. For a polymer of N monomers, a subsection of p monomers will relax in space in the same manner as a polymer of p monomers [6]. Therefore we consider the relaxation modes of each subchain of the polymer and label them with the indices $p = 1, 2, ..., N$. Each mode has a corresponding relaxation time that obeys the relation

$$\tau_p \sim \left(\frac{N}{p}\right)^{\beta}, \tag{2.7}$$

where the scaling exponent β depends on solvent quality and the presence of hydrodynamic (HD) interactions. When HD interactions are excluded, $\beta = 1 + 2\nu$, and $\beta = 3\nu$ when they are included [6].

To experimentally determine these relaxation times, the normalized time autocorrelation function $C(t)$ is used:

$$C(t) = \frac{\langle x(t_0 + t)x(t_0)\rangle - \langle x_0\rangle^2}{\langle x^2\rangle - \langle x\rangle^2}, \tag{2.8}$$

where $x(t)$ is a randomly fluctuating quantity, t_0 is some initial time and t is the time interval over which the correlation function is being calculated. For $t = 0$, there is

exact correlation so $C(0) = 1$, while in the limit $t \to \infty$, the quantities $x(t_0)$ and $x(t + t_0)$ become completely uncorrelated so $\lim_{t\to\infty} C(t) = 0$. In accord with these two limiting cases, the correlation function often takes the form

$$C(t) = e^{-t/\tau}, \tag{2.9}$$

where τ is called the correlation time, or the time required for the quantity in question to become uncorrelated. In the context of polymer dynamics, the fluctuating quantities are R_e and R_g and the correlation function is a linear combination of exponentials corresponding to the N relaxation modes: [6]

$$C(t) = \sum_{p=1}^{N} a_p e^{-t/\tau_p}, \tag{2.10}$$

where a_p are constants that depend on the details of the model. In practice, we generally observe a single component of the end-to-end displacement $R_{e,\alpha}$ and consider long times by which the $p = 1$ term dominates:

$$C_{e,\alpha}(t) \approx a_1 e^{-t/\tau_{e,\alpha}}, \tag{2.11}$$

where $\tau_{e,\alpha}$ is the longest relaxation time for the end-to-end displacement along the α-axis. This quantity is taken to be the polymer relaxation time in that dimension, as it provides the most accurate measure of the time required for the chain conformation to become uncorrelated with itself.

2.2 Polymer Translocation

As established in Section 1.3, polymer translocation involves the transport of a polymer through a nanopore. To measure the rate of this process, we call the time taken for the complete emptying of the nanopore the translocation time τ. Of great interest in the study of translocation is how the mean translocation time scales with chain length, or $\tau \sim N^{\alpha}$. A number of theoretical approaches have been proposed for determining the α scaling exponent, and it has been a topic of considerable debate over the years. Some of these approaches begin by assuming that translocation is sufficiently slow so that the *cis* and *trans* chain segments remain in conformational equilibrium during the process. Mathematically, this can be described as

$$\tau \gg \tau_r. \tag{2.12}$$

That is to say, the mean translocation time is much larger than the relaxation time of the chain. This condition is exhibited in the aptly named quasi-equilibrium regime.

Taking the assumption of quasi-equilibrum, Sung and Park [50], and later Muthukumar [51], employed the Fokker-Planck (FP) formalism to make theoretical predictions for the scaling exponent α. In the case of a small chemical potential difference $\Delta\mu$ across the pore (unbiased translocation), Muthukumar arrived at $\tau \sim N^2$ — representative of simple diffusion. Chuang et al. [52] challenged the scaling exponent of $\alpha = 2$, claiming that the lower limit for unbiased translocation should be set by the Rouse time (slowest relaxation time in absence of HD interactions) as $\tau \sim N^{1+2\nu}$. Their prediction has been supported by numerous simulations in 2D and 3D, [31, 53–56], but several other subsequent/concurrent studies found exponents of around $2 + \nu$ for

Rouse, and $1 + 2\nu$ for Zimm polymers (HD interactions included) [34, 57–59].

In the case of driven or biased translocation, FP theory dictates that translocation time scales as $\tau \sim N/\Delta\mu$ for a sufficiently large chemical potential difference (or driving force) across the pore [50, 51]. For out-of-equilibrium biased translocation in the presence of hydrodynamics and good solvent conditions, Vocks et al. [60] suggested $\alpha = 3\nu/(1 + \nu) \approx 1.125$ based on chain memory effects due to local tension in the polymer when a monomer translocates from one side to the other. Some simulation studies of biased translocation with HD have reported scaling exponents close to this value [43, 61] including a 2010 DPD study by Kapahnke et al. [34]. It was recently demonstrated by Ikonen et al. [62] that α has a large dependence on chain length, and approaches the asymptotic limit $\alpha = 1 + \nu$ at very large N. Additionally the authors found that by decreasing N and increasing pore friction, the scaling exponent approached $\alpha = 1$, coinciding with the FP prediction for a sufficiently strong driving force.

Evidently, the exponent debate has not been settled, but in the case of quasi-equilibrium the original Fokker-Planck predictions of $\tau \sim N^2$ for unforced translocation, and $\tau \sim N$ for forced, are expected to emerge. Recent work by de Haan and Slater [35] showed that at high solvent viscosity, corresponding to a long polymer relaxation time τ_r, the scaling exponent for unbiased translocation was close to $\alpha = 2 + \nu$, while at low viscosity and short τ_r, the value approached $\alpha = 2$. This suggests that the FP prediction is valid for sufficiently fast subchain relaxation. As an alternative to decreasing solvent viscosity, the quasi-equilibrium regime can be reached by a sufficient increase in pore friction [63]. In this way, subchain relaxation remains constant while

translocation time increases, so the condition of Eq. (2.12) is still satisfied.

Since the pore used in this study is of finite length, we also measure the first passage time τ_1, as the time required for all monomers to have emptied from either the *cis* or *trans* reservoirs. In practice, we expect the two translocation times to differ very little and to follow the same scaling relations. We mainly focus on the emptying time τ, but consider τ_1 when comparing our results with FP predictions.

For the remainder of this section, we begin by introducing a coordinate to quantify translocation, then we explore the idea of an entropic barrier governing the translocation process. Finally, we review the aforementioned Fokker-Planck formalism for predicting translocation time distributions.

2.2.1 Translocation Coordinate

Consider a polymer translocating through a nanopore aligned along the z-axis between $z = 0$ and $z = L_p$. In order to quantify the degree of translocation, we define the translocation coordinate Q as

$$Q = \frac{1}{N} \sum_{i=1}^{N} Q_i, \tag{2.13}$$

where N is the number of monomers, Q_i is the translocation coordinate for the ith monomer given by

$$Q_i = \begin{cases} 0, & z_i < 0 \\ z_i/L_p, & 0 < z_i < L_p \\ 1, & z_i > L_p, \end{cases} \tag{2.14}$$

and z_i is the z coordinate of monomer i.

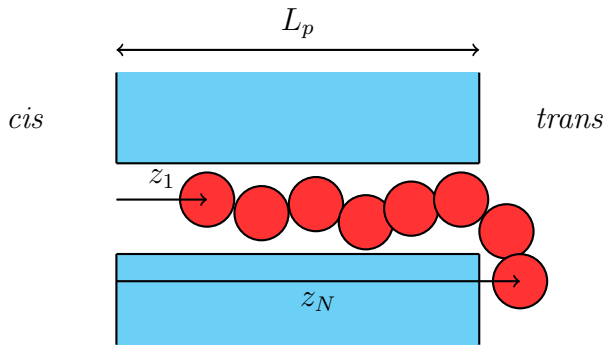

Figure 2.2: A two dimensional drawing of a polymer consisting of $N = 8$ monomers translocating through a pore of length L_p.

Clearly, Q lies in the range $[0, 1]$. $Q = 0$ when the polymer is completely on the *cis* side of the pore, $Q = 1$ when the polymer is completely on the *trans* side of the pore, and $0 < Q < 1$ if there are any monomers in the pore. For example, in Figure 2.2 the first monomer is in the pore with $0 < Q_1 < 1$, while the last monomer is on the trans side of the pore with $Q_N = 1$.

This choice of translocation coordinate has the advantage of being a continuous quantity, compared to other simulation studies [52, 64] which use the discrete quantity s - defined as the number of monomers on the *trans* side of the pore.

2.2.2 Thermodynamics and Free Energy Profiles

For a system in the canonical ensemble, the number of particles N, the volume V and the temperature T are fixed. For this reason, it is also called the NVT ensemble. An important quantity when studying these systems is the Helmholtz free energy, defined

$$F = U - TS, \tag{2.15}$$

where U is the total average energy, T is the system temperature and S is the entropy. For this study, S is effectively the configurational entropy of the polymer and is a measure of the number of conformations or microstates Ω available to the chain. Mathematically, this is expressed as

$$S = k_B \ln \Omega, \tag{2.16}$$

where k_B is the Boltzmann constant.

In the context of polymer translocation, the free energy is parameterized by the degree of translocation:

$$F(Q) = U(Q) - TS(Q). \tag{2.17}$$

When the polymer is confined in the pore ($0 < Q < 1$), it has less space to spread out and fewer conformations available to it, so consequently it has lower configurational entropy. From the above equation, this clearly leads to an increase in free energy. The free energy function is also given by

$$F(Q) = -k_B T \ln Z(Q), \tag{2.18}$$

where $Z(Q)$ is the configurational partition function of the polymer corresponding to the given value of Q. The complete partition function has a kinetic factor that is omitted here because it does not depend on Q. Generally, it is favourable for the polymer to be located outside of the pore (high or low values of Q). This is associated with an energy barrier arising from loss of configurational entropy due to the geometric constriction of the pore, and the chain must overcome this entropic barrier to successfully translocate.

An analytical approximation of the free energy barrier can be made by first considering the partition function of a self-avoiding chain (monomers cannot occupy the same space) in good solvent with one end tethered to a hard wall [65]:

$$Z = N^{\lambda-1} e^{-\mu N/k_B T}, \tag{2.19}$$

where μ is the chemical potential per monomer and the scaling exponent λ has been shown to be $\lambda \approx 0.69$ for a self-avoiding flexible polymer [66]. For a polymer translocating through a nanopore of zero length, the *cis* and *trans* subchains have corresponding partition functions Z_c and Z_t of the same form as Eq. (2.19) [14]. The overall configurational partition function is thus a product of the two:

$$Z(m) = Z_c(N-m) Z_t(m), \tag{2.20}$$

where m is the number of monomers on the *trans* side of the pore and serves as discrete measure of translocation. The system is illustrated in Figure 2.3.

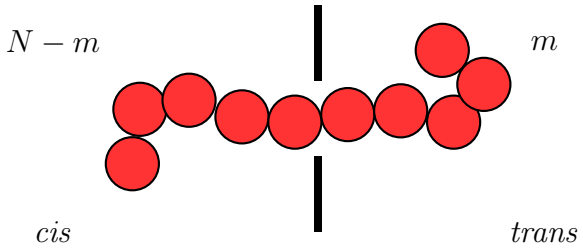

Figure 2.3: A polymer consisting of $N = 10$ monomers translocating through a nanopore of vanishing length. The labelled quantities are the number of monomers on their respective sides.

Now applying Eq. (2.18) and ignoring unnecessary constant terms gives the free energy function of the translocating polymer [14]:

$$\frac{F(m)}{k_B T} = (1 - \lambda) \ln[(N - m)(m)] - m\frac{\Delta\mu}{k_B T}, \tag{2.21}$$

where $\Delta\mu$ is the difference in monomer chemical potential between the *cis* and *trans* regions. Since the pore is of infinitesimal length, the discrete quantity m in Eq. (2.21) can be easily interchanged with the translocation coordinate by the relation $Q = m/N$.

With the above approximation, the entropic barrier can now be visualized in Figure 2.4. The polymer experiences a free energy minimum at the beginning (a) and end (c) of translocation, and a maximum during translocation (b). From the plot of the resulting free energy profile (d), the aforementioned free energy barrier impeding translocation is clearly seen. The symmetrical black curve is representative of unbiased translocation ($\Delta\mu = 0$), while the asymmetrical red curve shows the effect of a rather small chemical potential difference between the *cis* and *trans* sides of the pore.

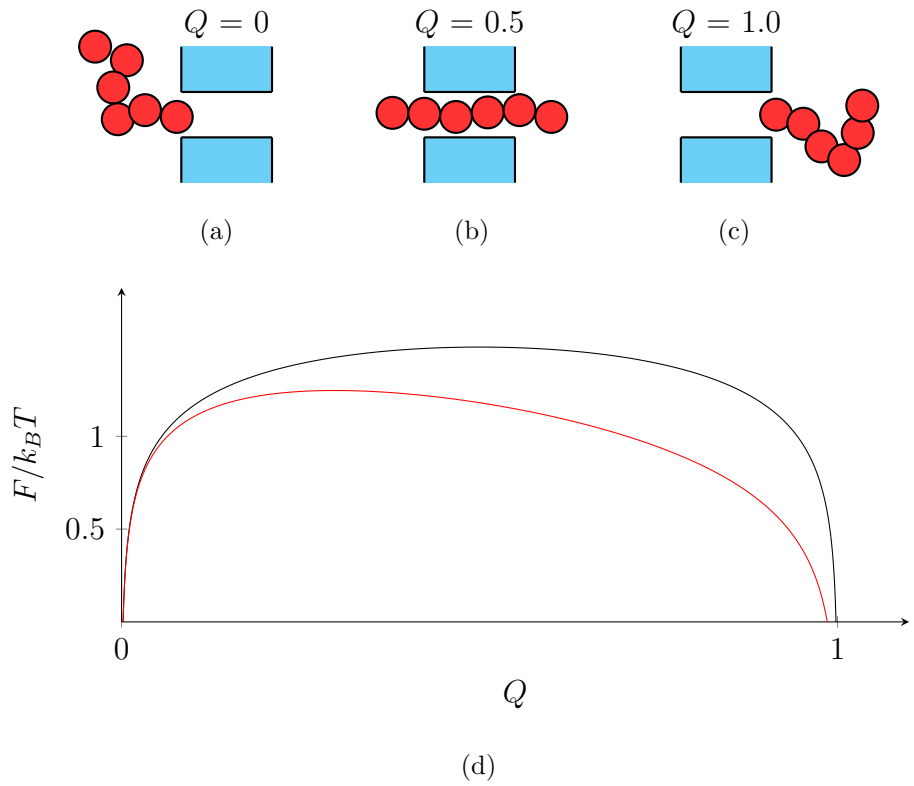

Figure 2.4: (a-c) Different stages of translocation. (d) The approximate free energy function as per Eq. (2.21) with $\Delta\mu = 0$ in black and $\Delta\mu = k_BT/10$ in red.

2.2.3 Fokker-Planck Formalism

Assuming quasi-equilibrium, one can make predictions for translocation time based on the related free energy function $F(Q)$. The time-dependent translocation probability distribution $P(Q,t)$ is governed by the Fokker-Planck equation [14]:

$$\frac{\partial P(Q,t)}{\partial t} = \frac{\partial}{\partial Q}\left(\frac{D}{k_BT}\frac{\partial F}{\partial Q}P(Q,t)\right) + \frac{\partial}{\partial Q}D\frac{\partial P(Q,t)}{\partial Q}, \tag{2.22}$$

where D is an effective diffusion coefficient given by the Einsteinian relation:

$$D = \frac{k_B T}{\gamma_{\text{pol}}}, \tag{2.23}$$

where γ_{pol} is the overall friction coefficient of the entire polymer. In the limit of sufficiently high pore friction, however, the friction experienced by the polymer is dominated by the monomers inside the nanopore. Defining N_{eff} as the effective number of monomers whose dynamics is governed by pore friction, we approximate the polymer coefficient as

$$\gamma_{\text{pol}} = N_{\text{eff}} \gamma_{\text{pore}}, \tag{2.24}$$

where γ_{pore} is the dissipative force strength inside the nanopore, and will be explained in context of our model in Section 4.3.2.

Now to apply the Fokker-Planck equation, we consider a domain bounded by $Q = Q_a$ and $Q = Q_b$. The first passage time τ for a polymer located at $Q_0 \in [Q_b, Q_a]$ at time $t = 0$ to reach either boundary has a probability distribution given by [14]

$$g(\tau; Q_0) = -\frac{d}{d\tau} \int_{Q_a}^{Q_b} dQ \; p(Q, \tau; Q_0, 0), \tag{2.25}$$

where $p(Q, t; Q', t')$ is the conditional probability that the polymer reaches the value Q at time t given that it has the value Q' at the earlier time t'. Setting $Q_a = 0$ and $Q_b = 1$ gives us the probability distribution for a successful translocation event, in which the nanopore has completely emptied.

Chapter 3

Methods

In this study, two simulation techniques were used: dissipative particle dynamics (DPD) and Metropolis Monte Carlo (MC). The former was used to study dynamical properties of the system, and the latter for non-dynamical properties (specifically the free energy). Both are briefly described in this chapter, as well as the multiple-histogram method, which was used in conjunction with the Monte Carlo technique to calculate variation of the free energy with translocation coordinate.

3.1 Dissipative Particle Dynamics

Dissipative particle dynamics is a mesoscopic simulation method that has become quite popular as an alternative to conventional microscopic molecular dynamics (MD). DPD has been shown to fully incorporate hydrodynamic behaviour without the high computational cost of the MD method, making it preferable for simulations involving long time and length scales [29, 67–69]. The method was first introduced by Hoogerbrugge and Koelman [70] for simulating complex isothermal fluids, then revised by

Español and Warren [71] who derived the Fokker-Planck equation for the method and the corresponding fluctuation-dissipation theorem. The following is a less detailed summary of the method than that given by Groot and Warren [72].

As a coarse-grained technique, DPD involves representing complex molecules as soft spherical beads connected with springs which interact through three pairwise interactions: the conservative force $\vec{F}^{\mathrm{C}}$, the dissipative force $\vec{F}^{\mathrm{D}}$ and the random force $\vec{F}^{\mathrm{R}}$. The ith particle of the system thus has a total non-bonded force $\vec{f}_i$ given by

$$\vec{f}_i = \sum_{j \neq i} (\vec{F}^{\mathrm{C}}_{ij} + \vec{F}^{\mathrm{D}}_{ij} + \vec{F}^{\mathrm{R}}_{ij}), \tag{3.1}$$

where the sum runs over all the other particles within a given cutoff radius r_c. Moreover, a particle j does not interact with the particle i if the separation between the two is greater than r_c. It is convenient to set the cutoff radius to unity ($r_c = 1$) to define the length scale in these simulations.

The conservative force is a soft repulsive interaction acting along the line connecting the particle centres. The typical choice, and the one used in this study, is given by

$$\vec{F}^{\mathrm{C}}_{ij} = \begin{cases} a_{ij}(1 - r_{ij})\hat{r}_{ij}, & r_{ij} < r_c \\ \vec{0}, & r_{ij} \geq r_c, \end{cases} \tag{3.2}$$

where a_{ij} is the maximum repulsion between particles i and j, $\vec{r}_{ij} = \vec{r}_i - \vec{r}_j$, $r_{ij} = |\vec{r}_{ij}|$, and $\hat{r}_{ij} = \vec{r}_{ij}/|\vec{r}_{ij}|$. This is considered a soft interaction because it allows particles to overlap with each other. Of course, this is not physically realistic on the atomistic scale as it violates the Pauli exclusion principle, but since DPD is a coarse-grained

method, each particle represents and behaves as groups of atoms and molecules. This is different from a microscopic simulation method which must employ hard forces to prevent particle overlap.

The other forces are the dissipative force:

$$\vec{F}_{ij}^{\mathrm{D}} = -\gamma w^{\mathrm{D}}(r_{ij})(\hat{r}_{ij} \cdot \vec{v}_{ij})\hat{r}_{ij}, \tag{3.3}$$

which acts as the drag or friction, and the random force:

$$\vec{F}_{ij}^{\mathrm{R}} = \sigma w^{\mathrm{R}}(r_{ij})\xi_{ij}\hat{r}_{ij}, \tag{3.4}$$

which serves as the thermal fluctuations in the system. The γ and σ parameters control the strength of the dissipative and random forces respectively, ξ_{ij} is a randomly fluctuating in time variable with Gaussian statistics, the weighting functions w^{D} and w^{R} are distance-dependent and non-zero for $r_{ij} < r_c$, and $\vec{v}_{ij} = \vec{v}_i - \vec{v}_j$. As shown by Español and Warren [71], these two forces are intrinsically coupled, as any heat generated by the random fluctuations must be allowed to dissipate. This is encapsulated by the DPD fluctuation-dissipation theorem:

$$\sigma^2 = 2k_B T\gamma, \tag{3.5}$$

$$[w^R(r_{ij})]^2 = w^D(r_{ij}), \tag{3.6}$$

where k_B is the Boltzmann constant and T is the equilibrium temperature of the system. Eq. (3.5) relates the strengths of the forces, and also fixes the system temperature. In this way, the relation acts as a sort of thermostat for the system. Furthermore, Eq.

(3.6) implies that the one of the weighting functions is fixed by the arbitrary choice of the other. We follow the simple choice of Groot and Warren [72] for the form of the weighting functions:

$$w^D(r_{ij}) = [w^R(r_{ij})]^2 = \begin{cases} (1 - r_{ij}/r_c)^2, & r_{ij} < r_c \\ 0, & r_{ij} \geq r_c, \end{cases} \tag{3.7}$$

which has the same distance dependence as that in the conservative force.

To those familiar with it, the DPD method bears strong resemblance to the Langevin dynamics method, specifically the use of drag and random forces. A significant distinction is that the particular forms of the dissipative and random forces ensure that momentum is conserved locally with the DPD method [29]. As such, the correct hydrodynamic behaviour is recovered on sufficiently long length and time scales [73].

3.2 Metropolis Monte Carlo

In the canonical ensemble, the number of particles N, temperature T and volume V are constant. A microstate is a specific system configuration defined by the set of positions and momenta of all the particles:

$$(\vec{r}^N, \vec{p}^N) = (\vec{r}_1, \ldots, \vec{r}_N, \vec{p}_1, \ldots \vec{p}_N). \tag{3.8}$$

The probability of the system assuming this specific state is given by the Boltzmann distribution:

$$P(\vec{r}^N, \vec{p}^N) \propto \exp\left[-\beta E(\vec{r}^N, \vec{p}^N)\right], \tag{3.9}$$

which is normalized by integrating over all states:

$$P(\vec{r}^N, \vec{p}^N) = \frac{\exp\left[-\beta E(\vec{r}^N, \vec{p}^N)\right]}{\int \mathrm{d}^{3N}\vec{r}\, \mathrm{d}^{3N}\vec{p}\, \exp\left[-\beta E(\vec{r}^N, \vec{p}^N)\right]}, \tag{3.10}$$

where $\beta = 1/k_B T$ and the energy can be split into potential and kinetic energy as follows:

$$E(\vec{r}^N, \vec{p}^N) = U(\vec{r}^N) + K(\vec{p}^N). \tag{3.11}$$

With the energy separated, Eq. (3.10) can be integrated over momentum to yield the position probability distribution:

$$P(\vec{r}^N) = \int \mathrm{d}^{3N}\vec{p}\, P(\vec{r}^N, \vec{p}^N), \tag{3.12}$$

which can be shown to reduce to

$$P(\vec{r}^N) = \frac{\exp\left(-\beta U(\vec{r}^N)\right)}{\int \mathrm{d}^{3N}\vec{r}\, \exp[-\beta U(\vec{r}^N)]}. \tag{3.13}$$

Now consider a position-dependent quantity $A(\vec{r}^N)$. The ensemble average of A is

$$\langle A \rangle = \int \mathrm{d}^{3N}\vec{r}\, A(\vec{r}^N) P(\vec{r}^N) = \frac{\int \mathrm{d}^{3N}\vec{r}\, A(\vec{r}^N) \exp\left[-\beta U(\vec{r}^N)\right]}{\int \mathrm{d}^{3N}\vec{r}\, \exp\left[-\beta U(\vec{r}^N)\right]}. \tag{3.14}$$

Solving this integral is nigh impossible, but numerical techniques can be used to make approximations. One such technique is Metropolis Monte Carlo, which will be the focus of the remainder of this section.

At its core, the MC computational method involves randomly generating and sampling states of the system with probability governed by Eq. (3.13). For convenience, we start by introducing the state label:

$$\alpha \equiv \left\{\vec{r}^N\right\}. \tag{3.15}$$

Now summing over many states can give an approximate average of A:

$$\langle A \rangle \approx \frac{1}{N_s} \sum_{i=1}^{N_s} A(\alpha_i), \tag{3.16}$$

where the accuracy increases with the number of states sampled N_s, and becomes exact in the limit $N_s \to \infty$. The Metropolis method involves the use of a Markov chain, by which each state in the sequence depends only on the previous element:

$$\alpha_1 \to \alpha_2 \to \alpha_3 \to \cdots \to \alpha_{N_s}, \tag{3.17}$$

where the subscripts refer to the order in which the algorithm generates the states. In order to ensure the probability by which a given state is visited does not change with time, the following balance condition must be satisfied:

$$\sum_b P(a)W(a \to b) = \sum_b P(b)W(b \to a), \tag{3.18}$$

where $P(a)$ is the probability of state a occurring and $W(a \to b)$ is the conditional probability that the system evolves to state b given it is already in state a. Alternatively, a sufficient but unnecessary condition is that of detailed balance:

$$P(a)W(a \to b) = P(b)W(b \to a), \tag{3.19}$$

which can be rearranged as

$$\frac{W(a \to b)}{W(b \to a)} = \frac{P(b)}{P(a)}. \tag{3.20}$$

Now recalling Eq. (3.13), we have

$$\frac{W(a \to b)}{W(b \to a)} = \exp[-\beta(U(b) - U(a)]. \tag{3.21}$$

From a state a, let $P_{\text{trial}}(a \to b)$ be the conditional probability that a new trial state b is generated by the algorithm, and let $P_{\text{acc}}(a \to b)$ be the probability that the move is accepted. So we have

$$W(a \to b) = P_{\text{trial}}(a \to b)P_{\text{acc}}(a \to b). \tag{3.22}$$

We now choose the following condition to be true:

$$P_{\text{trial}}(a \to b) = P_{\text{trial}}(b \to a). \tag{3.23}$$

That is to say, the probabilities of the system progressing from state a to b, and vice versa, are equal. Now combining Eqs. (3.21), (3.22) and (3.23) gives the Boltzmann factor:

$$\frac{P_{\text{acc}}(a \to b)}{P_{\text{acc}}(b \to a)} = \exp[-\beta(U(b) - U(a)] = \exp[-\beta\Delta U]. \tag{3.24}$$

To apply this condition to our simulations, we start with the system in a random microstate a. We generate new states by randomly choosing a single particle with position $\vec{r}_0$ and displacing it by an amount $\vec{d}$ to get the trial position $\vec{r}_t$:

$$\vec{r}_t = \vec{r}_0 + \vec{d}. \tag{3.25}$$

In accord with Eq. (3.24), this new trial microstate b is then either accepted or rejected according to the following criteria:

$$P_{\text{acc}}(a \to b) = \begin{cases} 1, & U(b) \leq U(a) \\ \exp[-\beta(U(b) - U(a))], & U(b) > U(a). \end{cases} \tag{3.26}$$

Thus, a trial move is always accepted if it results in an energy reduction. Otherwise, the move is accepted with a probability given by the Boltzmann factor.

3.3 Multiple Histogram Method

For the Monte Carlo simulations of this study, the quantity of interest is the free energy $F(Q)$ and its variation with the translocation coordinate Q, as detailed in Section 2.2.1. Unfortunately, the implementation described in the previous section is inefficient at sampling the free energy barrier when the variation in F exceeds a few $k_B T$. One way to circumvent this problem is to employ the self-consistent histogram method (SCHM) [29].

We begin by implementing the following window potential:

$$W_i(Q) = \begin{cases} \infty, & Q < Q_i^{\min} \\ 0, & Q_i^{\min} < Q < Q_i^{\max} \\ \infty, & Q > Q_i^{\max}, \end{cases} \tag{3.27}$$

where $Q_i^{\min}$ and $Q_i^{\max}$ define the range of the ith window. Clearly a trial move that results in the polymer leaving this window will always be rejected, as per the condition in Eq. (3.26). In this way, a polymer simulated in this window is restricted to Q values between $(Q_i^{\min}, Q_i^{\max})$. Choice of window width ΔQ is small enough to ensure the variation in F does not exceed a few k_BT, and adjacent windows are allowed to overlap with each other by $\Delta Q/2$. Each window is then run in a separate simulation to generate individual window probability distributions $p_i(Q)$, which are combined to reconstruct the overall equilibrium probability distribution $P(Q)$ [29]. Now to calculate the free energy function, we note that the configurational partition function $Z(Q)$ of Eq. (2.18) is proportional to the number of conformations available to the polymer. Thus we can write the free energy as

$$F(Q) = -k_BT \ln P(Q). \tag{3.28}$$

With this equation and the probability distribution obtained from the SCHM method, it is then straightforward to construct translocation free energy profiles.

Chapter 4

Model

In this chapter, we discuss the details, merits and limitations of the molecular model used for the computer simulations. At its most fundamental level, we use an off-lattice coarse-grained model, but there are several important features that make it an appropriate choice for polymer translocation.

4.1 Polymer Model

In our simulations, the polymer is modelled as a bead-spring chain consisting of N DPD monomers. Consecutive monomers in the chain are bonded and interact via the finitely extensible nonlinear elastic (FENE) potential:

$$U_{\mathrm{FENE}}(r_{ij}) = \begin{cases} -\frac{K}{2}(r_{\max} - r_{\mathrm{eq}})^2 \ln\left[1 - \left(\frac{r_{ij} - r_{\mathrm{eq}}}{r_{\max} - r_{\mathrm{eq}}}\right)^2\right] & r_{ij} \leq r_{\max} \\ \infty & r_{ij} > r_{\max} \end{cases} \tag{4.1}$$

where K is the spring constant, $r_{\max}$ is the maximum bond length and r_{eq} is the equilibrium bond length. The FENE potential was chosen because it is widely used

and a well characterized potential for modelling bonds in polymeric systems [74]. Besides this interaction, each monomer is also subject to the standard DPD forces described by Eqs. (3.2)-(3.4).

4.2 Wall and Pore Model

The wall is modelled as three layers of frozen DPD particles on a lattice. These wall particles interact with monomers and solvent particles, but not with each other. The spacing between the particles is $r_{\text{wall}} = (\sqrt[3]{\rho_{\text{wall}}})^{-1}$ where ρ_{wall} is the chosen wall density.

To create the nanopore, a single particle in each layer of the wall is removed to form a narrow channel. Thus the pore is square with width $w_{\text{pore}} = 2r_{\text{wall}}$ and length $L_{\text{pore}} = 2r_{\text{wall}}$. As pictured in Figure 4.1, the pore was chosen to lie along the z-axis.

4.3 Pairwise Interactions

4.3.1 Conservative Force

For the DPD method, the principle interaction between all particles is the conservative force $\vec{F}_{ij}^{C}$ given by Eq. (3.2). The strength of the interaction is tuned by the a_{ij} parameter, where i and j refer to the particle types. Consequently, there is a strength parameter for each pair of types:

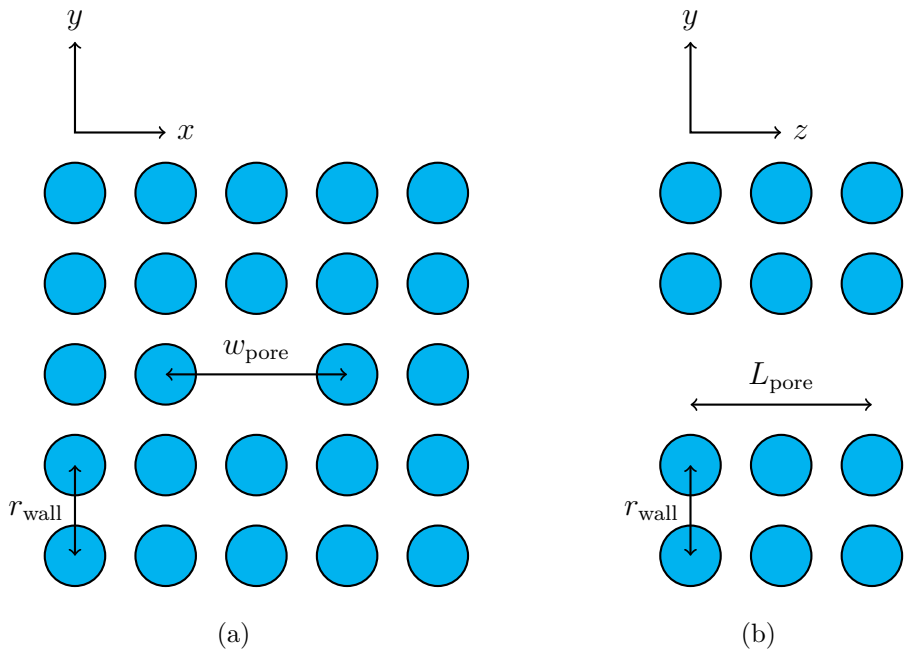

Figure 4.1: (a) A front view of the wall and nanopore. (b) A side view of the wall and nanopore. To distinguish between the reservoirs, the left and right side are labelled *cis* and *trans* respectively.

$$a_{ij} = \begin{cases} a_{\text{mm}}, & \text{monomer} - \text{monomer} \\ a_{\text{ms}}, & \text{monomer} - \text{solvent} \\ a_{\text{mw}}, & \text{monomer} - \text{wall} \\ a_{\text{ss}}, & \text{solvent} - \text{solvent} \\ a_{\text{sw}}, & \text{solvent} - \text{wall}. \end{cases} \tag{4.2}$$

The only pair omitted above is that between wall particles, as they do not interact with each other. Of particular importance here is the monomer-solvent interaction strength a_{ms}. As explained in Section 2.1.2, this parameter is related to solvent quality – a large value will cause the polymer chain to fold in on itself to a globular structure. One way to bias translocation direction is to have differing solvent qualities on either side of

the pore. Energetically, it is more favourable for the polymer to spread out and adopt a coil-like conformation, so translocation will be biased towards the better solvent. This can be done by dividing a_{ms} into two parameters: a_{cis} and a_{trans} for each side. The idea is depicted in Figure 4.2 (a).

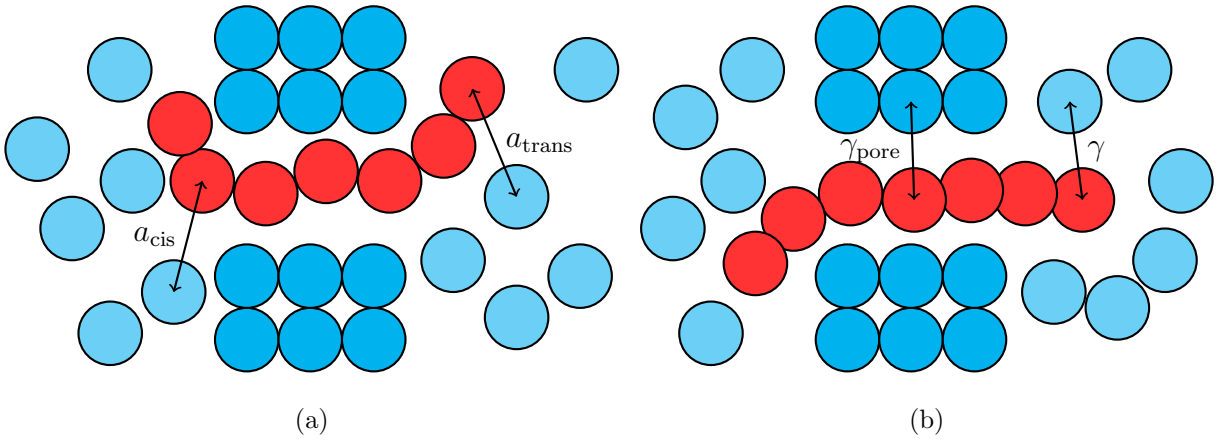

Figure 4.2: Side views of the polymer-nanopore system. (a) Labelled are the conservative force interactions between monomer and solvent particles on the *cis* and *trans* sides. (b) Labelled are the dissipative force interactions for monomers inside and outside the pore.

4.3.2 Dissipative Force

A significant factor controlling the rate of translocation, the dissipative force $\vec{F}_{ij}^{D}$ acts as a velocity dependent drag force and is given by Eq. (3.3). The γ coefficient controls the strength of this force, and it acts between all pairs of particle types. A distinction can be made, however, between the dissipative force inside and outside the pore. This is done by dividing the dissipative strength into γ and γ_{pore}. The latter tunes the strength of interaction between the monomers and the middle layer of pore particles (not the outer layers) and the former does the same for every other pair. The

difference is shown in Figure 4.2 (b). By increasing the γ_{pore} parameter, translocation can be effectively slowed without greatly affecting the relaxation time of the free ends of the chain in the solvent reservoirs. To account for this increase, a corresponding σ_{pore} is also chosen according to the DPD fluctuation-dissipative theorem from Eq. (3.5). It follows that this parameter controls the strength of the random force between monomers and the middle layer of pore particles.

4.4 Boundary Conditions

4.4.1 Simulation Box

To keep the system to a finite size, the particles are confined to a rectangular prism with side lengths L_x, L_y and L_z. In lieu of a bounding wall, periodic boundary conditions are employed at the edges of the simulation volume. When a particle reaches one of these edges, it is re-introduced at the opposite edge with the same velocity. The system can thus be thought of as a collection of periodic images as illustrated in Figure 4.3. In this way, particles may interact across boundaries with images of other particles within its cutoff distance. The use of periodic boundary conditions keeps the overall particle density constant while also avoiding surface effects that arise from introducing walls to the system, as we will soon discuss.

4.4.2 Wall

Despite its merits, the soft potentials employed in the mesoscopic DPD method do not prevent the DPD particles from penetrating the supposedly solid wall. As a result,

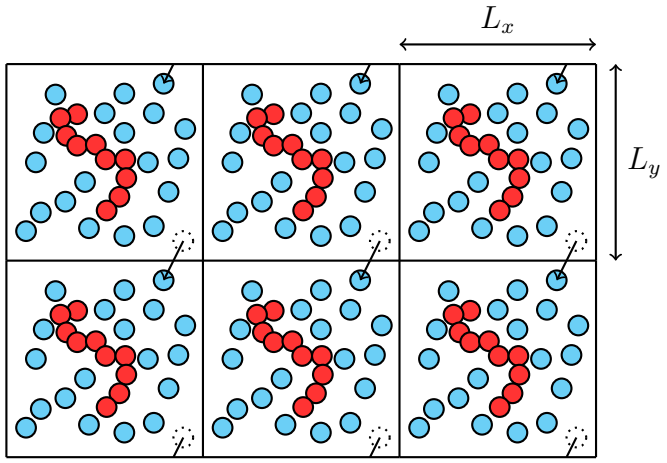

Figure 4.3: A two-dimensional depiction of periodic boundary conditions. The periodic images surround the simulation domain on all sides.

measures must be taken to ensure that monomers and solvent particles do not cross the solid-fluid interface. In addition to impenetrability, the wall should satisfy the no-slip condition, whereby particles at the boundary have zero velocity relative to the wall, without causing temperature and density fluctuations [75].

Several methods have been studied to treat the issue of boundary conditions in the DPD method. The Lees-Edward virtual boundary technique was one of the first, and used modified periodic boundary conditions without the need for an explicitly modelled wall [76]. This method has fallen out of favour, however, because it cannot be used for complex geometries. In its place, we follow Revenga et al. [77] who proposed the use of a wall of frozen DPD particles with reflections at the boundary. They compared and discussed various reflection mechanisms, including specular reflection, bounce-back reflection and Maxwellian reflection. In specular reflections, when a particle crosses the wall boundary, the normal component of its velocity is reversed while the tangential component does not change. Both are reversed in bounce-back reflections, causing the particle to return along the direction of incidence. Finally, in

Maxwellian reflections, the particles are reintroduced back into the fluid with velocity components following a Maxwellian distribution centred on the wall velocity. To evaluate the applicability of these mechanisms, the plane Couette flow was considered at different values of a dimensionless friction coefficient defined:

$$\tau \equiv \frac{\gamma\lambda}{dv_{\mathrm{T}}} \tag{4.3}$$

where γ is the familiar dissipative force coefficient, λ is the average distance between particles, d is the space dimension and v_{T} is the thermal velocity. For large values of τ, all three reflections satisfy the no-slip condition. For smaller values however, specular and Maxwellian reflections no longer satisfy no-slip, and bounce-back reflections show an anomalous temperature behaviour. Pivkin and Karniadakis [78] improved upon the bounce-back reflection method by analyzing the force per unit area exerted by all wall particles at different densities and proposed the following conservative repulsion between solvent and wall particles:

$$a_{\mathrm{sw}} = \frac{0.39(\rho_s + 0.1a_{\mathrm{ss}}\rho_s^2)}{0.0303\rho_{\mathrm{wall}}^2 + 0.5617\rho_{\mathrm{wall}} - 0.8536} \tag{4.4}$$

where ρ_s is the density of the solvent. It was shown that, in conjunction with bounce-back reflections, this particular form of a_{sw} satisfies the no-slip condition while minimizing density fluctuations around the boundary [49]. Accordingly, this is the bounce-back condition employed in our study.

4.5 Simulation Details

4.5.1 Reduced Units and System Parameters

As alluded to in Section 3.1, we take the convenient and conventional choice of $r_c = 1$ as the interaction cutoff radius, thereby defining the system's length scale. We also take the mass of each DPD particle to be $m = 1$, and work in units of energy set by the scale $k_BT = 1$. These choices stipulate that force be measured in units of k_BT/r_c and that time be measured in units of $\sqrt{mr_c^2/k_BT}$.

For our choice of key system parameters, we follow the standard values used in most DPD simulation studies [34, 46, 79–81]. We used $\rho_s = \rho_{\text{wall}} = 3$ as solvent and wall densities, with a timestep of $\Delta t = 0.04$. For the FENE potential of Eq. (4.1), we took spring constant $K = 40$, equilibrium bond length $r_{\text{eq}} = 0.7$, and maximum bond length $r_{\text{max}} = 2.0$. To avoid extremely large force values (and consequently program crashes) at separation distances close to r_{max}, a FENE cutoff distance was set at $r = 1.97$. After this value, the force levels off at $F_{\text{FENE}}(r = 1.97) \approx -100$. For the dissipative and random force strengths of Eqs. (3.3) and (3.4), we took $\sigma = 3$ and $\gamma = 4.5$ in accord with the fluctiation-dissipation theorem of Eq. (3.5) and to give a system temperature of $T = 1$. The conservative force coefficients of Eq. (4.2) were chosen to be $a_{\text{mm}} = a_{\text{ss}} = 25$ and $a_{\text{ms}} = 15$. This choice of $a_{\text{mm}} > a_{\text{ms}}$ represents good solvent conditions, as we will show in Section 5.1. Finally, using the values of ρ_s, ρ_{wall} and a_{ss}, we calculated $a_{\text{sw}} = 9.01$ using Eq. (4.4), and used the same for a_{mw}.

4.5.2 Free Polymer System

We began with the simple polymer in solvent system to examine the effects of solvent quality and test for hydroydynamics. The polymer was placed in a cubic simulation box with periodic boundary conditions and side length $5R_g$. This choice has been proven to minimize finite-size effects [46, 82].

To ensure good statistics, 50 DPD simulations were run for each different set of control parameters (chain length and solvent quality). At the beginning of each simulation, the polymer was initialized in an elongated configuration, then allowed to equilibrate for three times its relaxation time ($3\tau_r$). After the equilibration period, simulations ran for a time of $100\tau_r$ in order to study the dynamics on a timescale much longer than the chain relaxation time.

4.5.3 Polymer Translocation

Next we examined unbiased and biased translocation using both DPD and MC simulations. To minimize finite-size effects, we take the proven choice of $6R_g \times 6R_g \times 8R_g$ as simulation box dimensions [49]. The polymer was initially placed in a linear conformation with the middle monomer at the centre of the nanopore (odd numbers of monomers were used for symmetry). This monomer was also held fixed for a set time so that the chain could equilibrate. For the DPD simulations, this equilibration time was $3\tau_r$, while the MC system was allowed to equilibrate for 25% of the total number of cycles (an attempt to move a particle). The polymer was then released and translocation began.

The DPD simulations ended when the polymer completely exited to the *cis* or

trans reservoir, and the time passed was taken to be the translocation time τ. The MC simulations ended after 4×10^8 cycles. Typically, 200 DPD translocation simulations were run to find average translocation times, but as many as 1000 simulations were necessary to produce the first passage time distributions. A MC simulation was run for each of the 99 windows defined by Eq. (3.27) to generate free energy functions.

Chapter 5

Results and Discussion

In this chapter, we present and discuss the results of the DPD and MC computer simulations for the free polymer, unbiased translocation and biased translocation systems. For the most part, error bars for individual data points were omitted for clarity, but were used for weighting in the nonlinear least squares method for estimating fits to the data.

5.1 Free Polymer

Our first goal was to test for the presence of hydrodynamics – the most beneficial feature of the dissipative particle dynamics method. To do this, we studied a polymer immersed in different solvent conditions, measured mean radius of gyration and end-to-end displacement, and calculated chain relaxation time. Chain lengths of $N = 21$ to 51 were simulated, and the obtained quantities were then plotted versus number of bonds to test the relations of Eqs. (2.6) and (2.7). These equations hold in the limit of long polymer chains so are presented as scaling with number of monomers N, but

for short to intermediate chains (like in this study), the more appropriate choice is number of bonds $N-1$ [83].

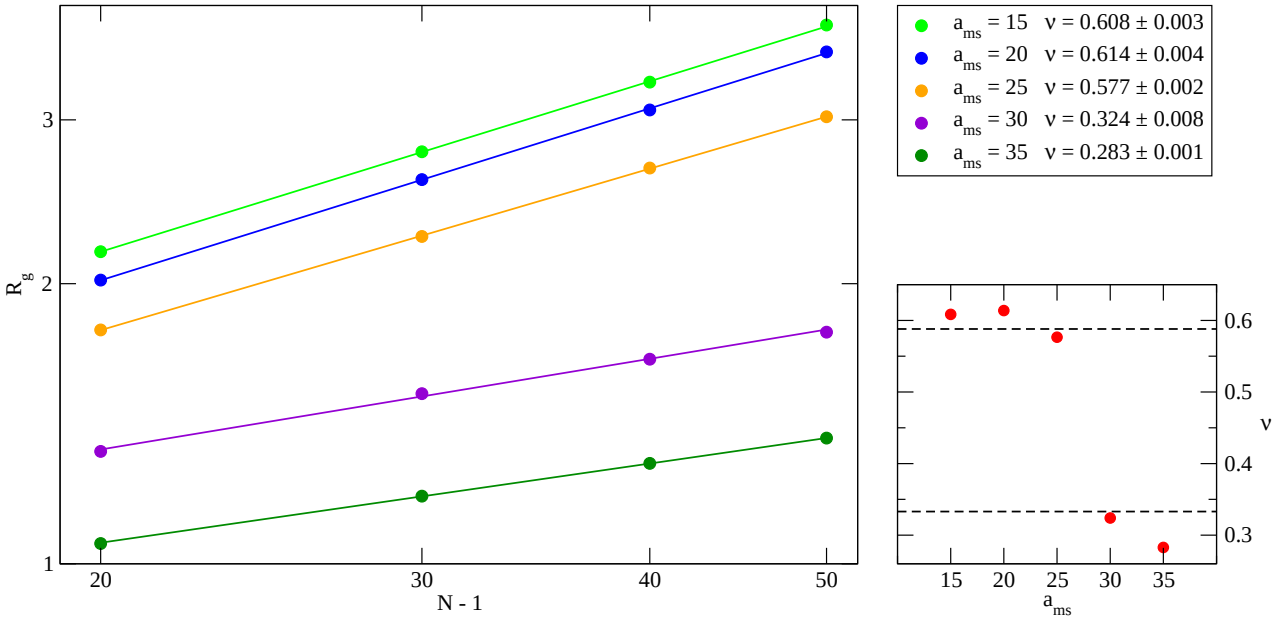

Figure 5.1: Mean radius of gyration vs. number of bonds for different solvent qualities, fit to the power law $R_g \sim (N-1)^{\nu}$. The subfigure shows the corresponding scaling exponents vs. monomer-solvent conservative force strength, and the dotted lines indicate expected values for good solvent ($\nu \approx 0.588$) and poor solvent conditions ($\nu = 1/3$).

Figure 5.1 shows how radius of gyration scales with number of bonds as the monomer-solvent conservative force strength (solvent quality) is varied. For the lower values of $a_{\text{ms}} = 15$, 20 and 25, values of the size exponent were found to be close to the predicted value for good solvent conditions. Beyond that, we see a crossover into poor solvent conditions. For $a_{\text{ms}} = 30$, we found a size exponent close to $\nu = 1/3$, suggesting that the polymer has taken a more compact globular shape. The tipping point between the qualities makes quantitative sense, as the monomer-monomer in-

teraction strength was kept constant at $a_{\mathrm{mm}} = 25$ for these simulations. Above that value, the higher a_{ms} makes it the dominant interaction and causes the monomers to aggregate together to form a globular structure as explained in Section 2.1.2. It is notable that the last point at $a_{\mathrm{ms}} = 35$ is quite a bit below the expected value for poor solvent conditions. This can perhaps be explained by the soft interactions of the coarse-grained DPD method allowing the polymer to collapse even further than anticipated in the case of hard potentials. To explore this further, higher values of a_{ms} should be tested to see if the size exponent decreases even more, or if it eventually levels out at a different value than 1/3. Other DPD studies investigating solvent quality did not find this anomaly, but varied solvent quality no higher than $a_{\mathrm{ms}} = 29$ [34] and 32 [45].

Conformational time auto-correlation functions were then calculated using the end-to-end displacement and fit to Eq. (2.11). Since we expect spherical symmetry in the case of a free polymer, the correlation functions for each axis were averaged to obtain the overall chain relaxation time τ_r. An example of this is shown in Figure 5.2. As expected, the components of the function are roughly the same within statistical fluctuations.

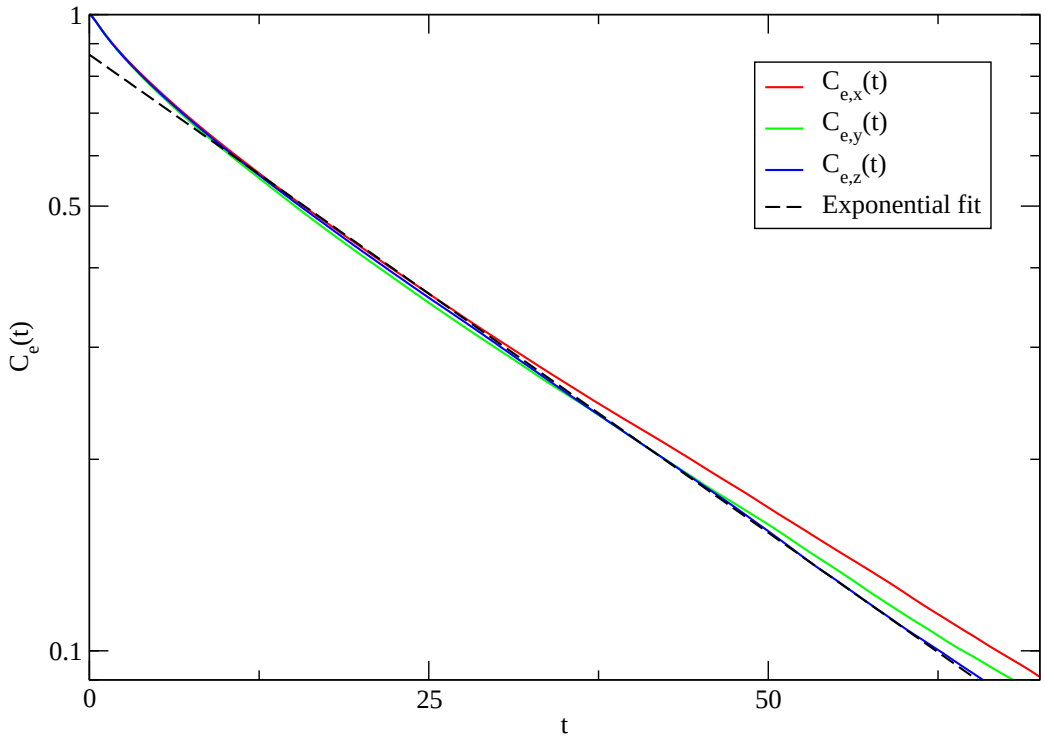

Figure 5.2: Conformational time auto-correlation functions calculated from R_e of a polymer of length $N = 41$ and $a_{\text{ms}} = 30$. The functions were averaged together and fit to an exponential decay for $t \geq 20$. The averaged chain relaxation time was found to be $\tau_r = 29.6 \pm 0.4$.

Relaxation times were calculated in this way for various polymer lengths and solvent qualities, and the results are presented in Figure 5.3. In the presence of hydrodynamic interactions and good solvent conditions, the scaling exponent is expected to be $\beta = 3\nu$. Thus for low monomer-solvent repulsion ($a_{\text{ms}} = 15, 20, 25$), our calculated values of the scaling exponent are consistent with the predicted $\beta \approx 3(0.588) = 1.746$. This suggests that hydrodynamic interactions are represented in our DPD model. For poor solvent conditions ($a_{\text{ms}} = 30$ and 35), the prediction $\beta = 3\nu$ is no longer meaningful so, unsurprisingly, the obtained scaling exponents in this regime were less than that value.

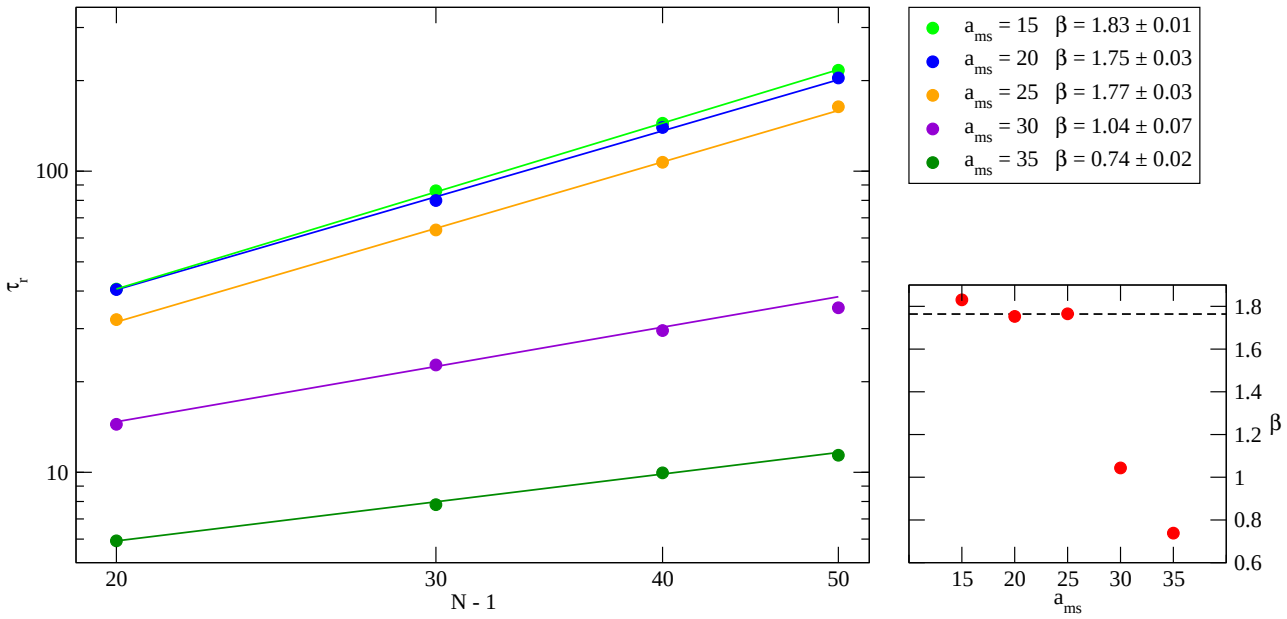

Figure 5.3: Chain relaxation time vs. number of bonds for various solvent qualities, fit to the power law $\tau_r \sim (N-1)^{\beta}$. The subfigure shows the corresponding scaling exponents vs. monomer-solvent conservative force strength, and the dotted line indicates the expected value for good solvent conditions in the presence of hydrodynamics ($\beta = 3\nu \approx 1.76$).

In this section, we have confirmed that our DPD model correctly exhibits hydrodynamic behaviour by examining how the chain relaxes in solvent. We have also shown that increasing the monomer-solvent conservative interaction strength causes the polymer to collapse to a globular structure, demonstrating a decline in solvent quality.

5.2 Polymer Translocation

Our goal for this section is to study unbiased and biased polymer translocation, and find the conditions that lead to the quasi-equilibrium regime. When this has been established, translocation time distributions can be compared to those given by the Fokker-Planck formalism to determine its validity in describing translocation dynamics. Before that can be done, we begin by examining how translocation time scales with polymer length, or $\tau \sim N^{\alpha}$. As with the free polymer scaling relations, however, we must make adjustments when considering these shorter chains. For finite-length nanopores, we instead consider how translocation time scales with effective length $N - N_p$, where N_p is the average number of monomers that lie inside a filled nanopore. For our purposes, we estimate this quantity as $N_p \approx L_p/\Delta z_p + 1$, where Δz_p is the average distance along z between bonded monomers inside the pore. With little variation, even in the case of biased translocation, we found $N_p \approx 3$ and accordingly used this value in analyzing the following data.

5.2.1 Unbiased

One way to approach quasi-equilibrium is to slow translocation rate by increasing pore friction. In this way, relaxation time of the subchains is unaffected while translocation time increases, thereby satisfying the equilibrium condition of Eq. (2.12). Figure 5.4 shows the scaling of τ with effective chain length for different values of the pore friction parameter γ_{pore}. As expected, increasing pore friction increases translocation time. For smaller values of the friction parameter ($\gamma_{\text{pore}} = 1$ and 4.5), the scaling exponent was found to be around 2.2, in agreement with the HD prediction of $\alpha = 1 + 2\nu$ in good

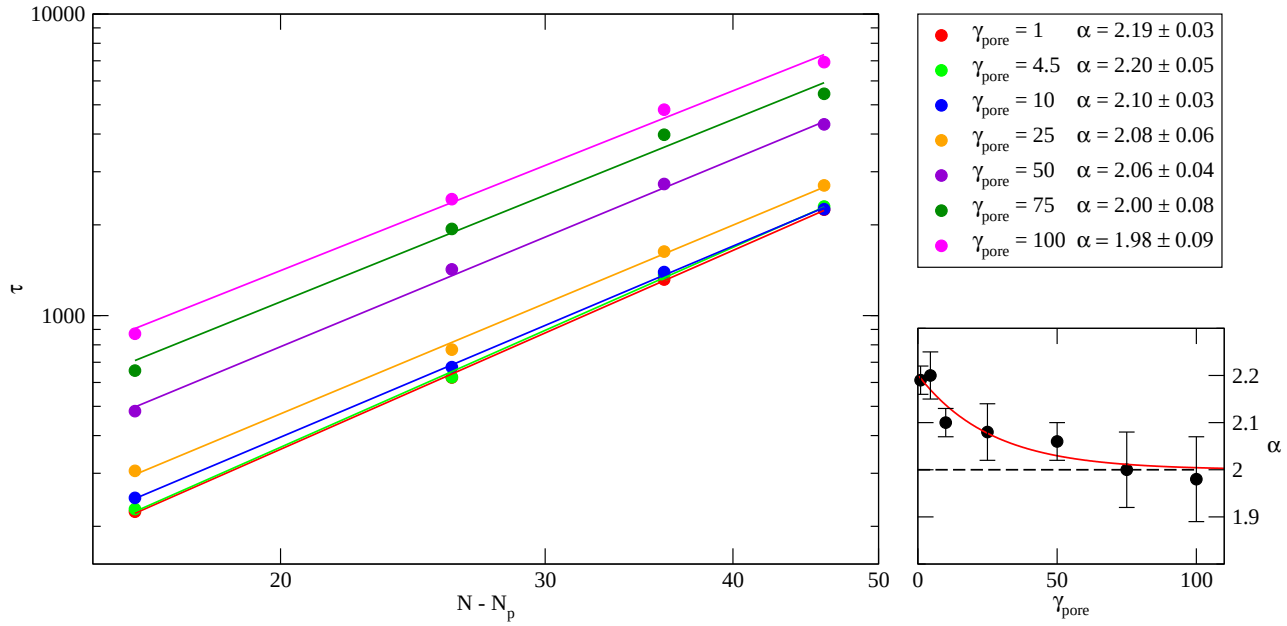

Figure 5.4: Mean translocation time vs. effective polymer length for various values of the pore friction coefficient, fit to the power law $\tau \sim (N - N_p)^{\alpha}$. The subfigure shows the corresponding scaling exponents vs. pore friction strength. The dotted line indicates the expected value in the quasi-equilibrium regime ($\alpha = 2$).

solvent conditions [52, 53, 55]. This again demonstrates the existence of hydrodynamic interactions with the DPD method. Increasing γ_{pore} causes a gradual decrease in the scaling exponent, finally reaching $\alpha = 2$ at the higher values of pore friction ($\gamma_{\text{pore}} =$ 75 and 100). This is the predicted value for the quasi-equilibrium regime, and is expected to hold as pore friction is increased even more. To ensure the asymptotic limit has been reached, however, higher pore friction strengths should be tested. In addition, more simulations of the presented data should be done to reduce statistical uncertainty.

It is also informative to plot mean translocation time against the pore friction parameter for different polymer lengths, as shown in Figure 5.5. In general, there are two sources of friction dictating the rate of translocation: friction of the polymer

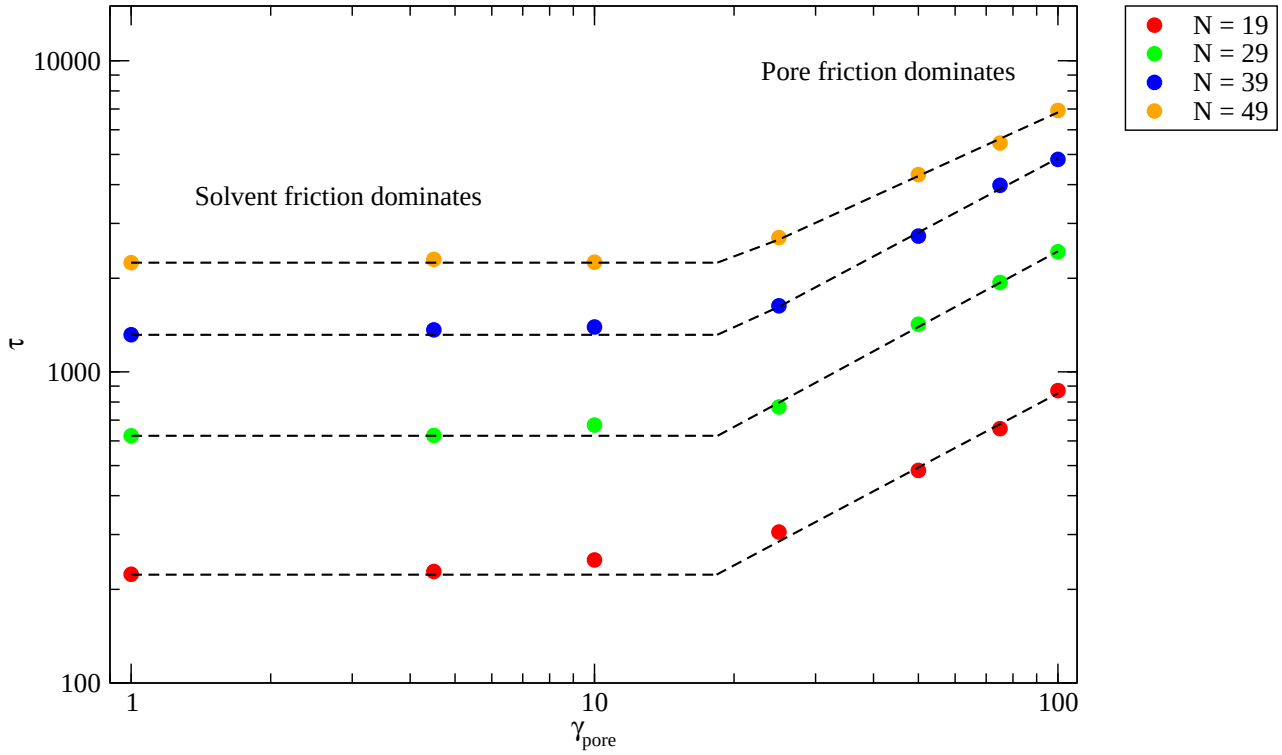

Figure 5.5: Mean translocation time vs. pore friction strength for various polymer lengths.

moving through the fluid (solvent friction) and friction from the restrictive aspects of the pore. Figure 5.5 shows a clear divide between the regimes where solvent friction dominates over pore and vice versa. The crossover seems to occur around a value of $\gamma_{\text{pore}} \approx 20$ and appears to be relatively consistent with polymer length (at least for the short lengths considered here). With this value in mind, we next tested predictions of the FP formalism.

Metropolis Monte Carlo simulations, along with the multiple histogram method to improve statistical efficiency, were first used to generate free energy profiles for polymer translocation. Although not particularly illuminating, Figure 5.6 exhibits certain characteristics we anticipate of unbiased translocation. The curve is symmetric, meaning translocation is not entropically favoured towards either the *cis* or *trans* reservoir.

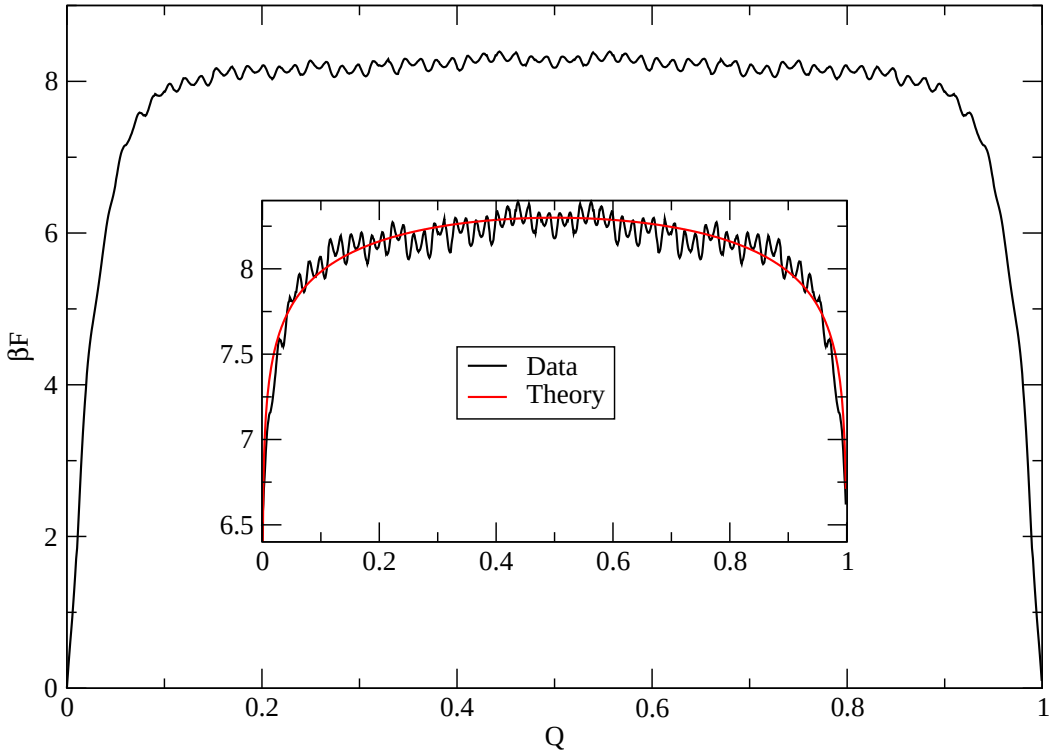

Figure 5.6: Free energy profile for a polymer of length $N = 31$ undergoing unbiased translocation through a pore of length $L_p = 2r_{\text{wall}} \approx 1.38$. The inset shows the same free energy function, but with the pore-emptying and pore-filling stages excluded. Overlaid in red for comparison is the theoretical function developed in Section 2.2.2.

The sharp decrease of the function on either side (high and low Q) correspond to the polymer exiting the pore, and is associated with an increase in the number of configurations available to the chain. Also as expected, free energy is at a maximum for $Q = 0.5$, and this maximum extends for values of Q corresponding to a filled pore. Although not tested in this study, a longer pore length should result in a proportional increase in the free energy barrier height [84]. The weak oscillations in the plateau section of the free energy likely arise due to the spacing between layers of pore particles, as seen in Figure 4.1. The period of oscillation is approximately $\Delta Q \approx 0.017$. For a polymer of length $N = 31$, this would correspond to an individual monomer

shifting by $\Delta Q_i \approx 0.52$ as per Eq. (2.13). Then multiplying by pore length gives monomer displacement $\Delta z_i \approx 0.72$, very close to the wall spacing $r_{\text{wall}} = 0.693$. Thus each oscillation is possibly a result of the monomers being repulsed by the equally spaced pore particles, making it more likely that the monomers are found between layers. We also compare the analytical approximation of Eq. (2.21) to the free energy function. For a finite length pore however, we only consider the free energy of the filled-pore stage during which friction experienced by the polymer remains constant [32]. Of course, the model used in deriving the analytical prediction does not give rise to the same oscillations; apart from that, we see excellent agreement between theory and simulation.

With these free energy functions parameterized by the translocation coordinate, the Fokker-Planck equation, Eq. (2.22), can now be used to to generate theoretical probability distributions for the first passage time τ_1. As shown previously, pore friction dominates translocation for values of $\gamma_{\text{pore}} > 20$, so we focus on values above that for our DPD simulations. Figures 5.7 and 5.8 show translocation time distributions for a $N = 31$ polymer at $\gamma_{\text{pore}} = 25$ and 50, respectively.

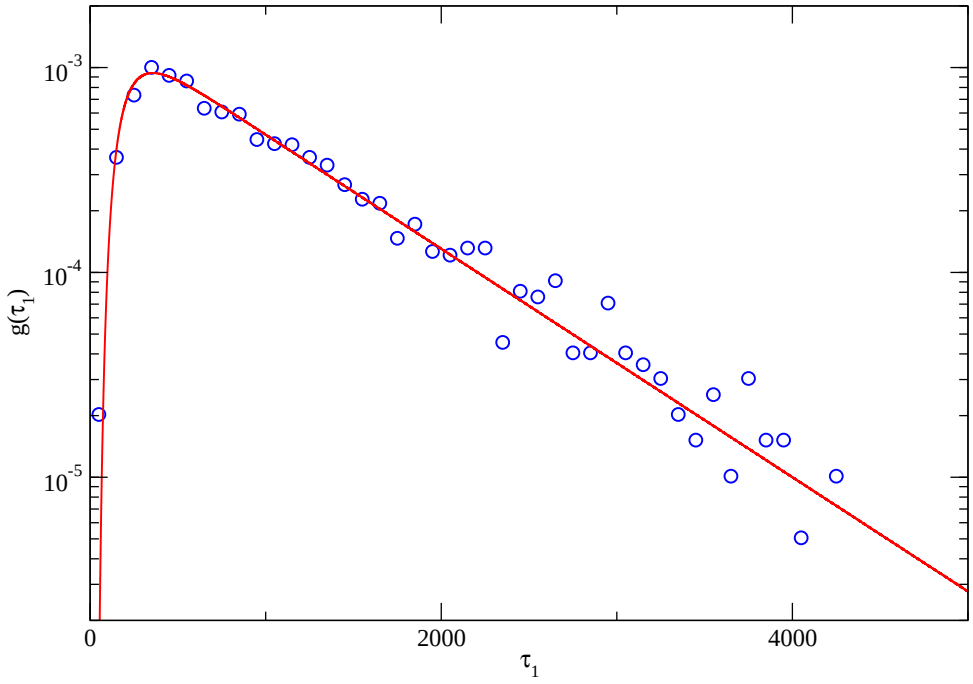

Figure 5.7: Unbiased translocation time distribution for a polymer of length $N = 31$ and $\gamma_{\text{pore}} = 25$ plotted on a log scale. The open circles represent DPD simulation data and the solid curves are FP theoretical predictions.

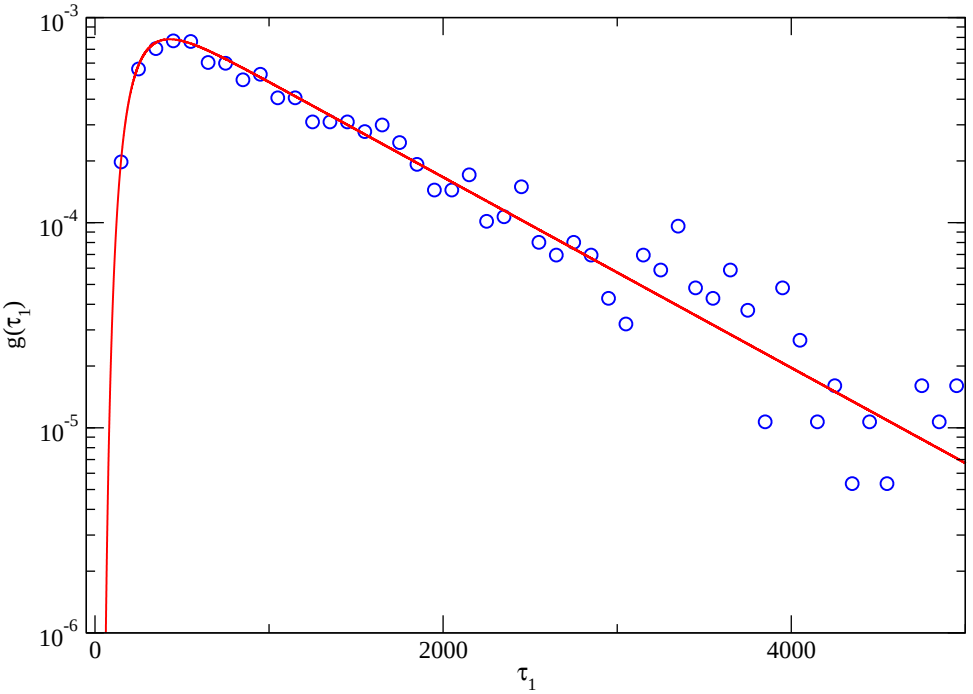

Figure 5.8: Unbiased translocation time distribution for a polymer of length $N = 31$ and $\gamma_{\text{pore}} = 50$ plotted on a log scale. The open circles represent DPD simulation data and the solid curves are FP theoretical predictions.

Evidently, there is clear agreement between the simulation data and the FP theory, suggesting that the pore friction is sufficiently high. Interestingly, these γ_{pore} values returned scaling exponents slightly higher than $\alpha = 2$ – the value indicative of quasi-equilibrium. We conclude that a good fit with the FP prediction does not necessarily imply quasi-equilibrum. A more thorough evaluation of translocation distributions at the higher values of pore friction (which yielded $\alpha \approx 2$) should help to elucidate this hypothesis.

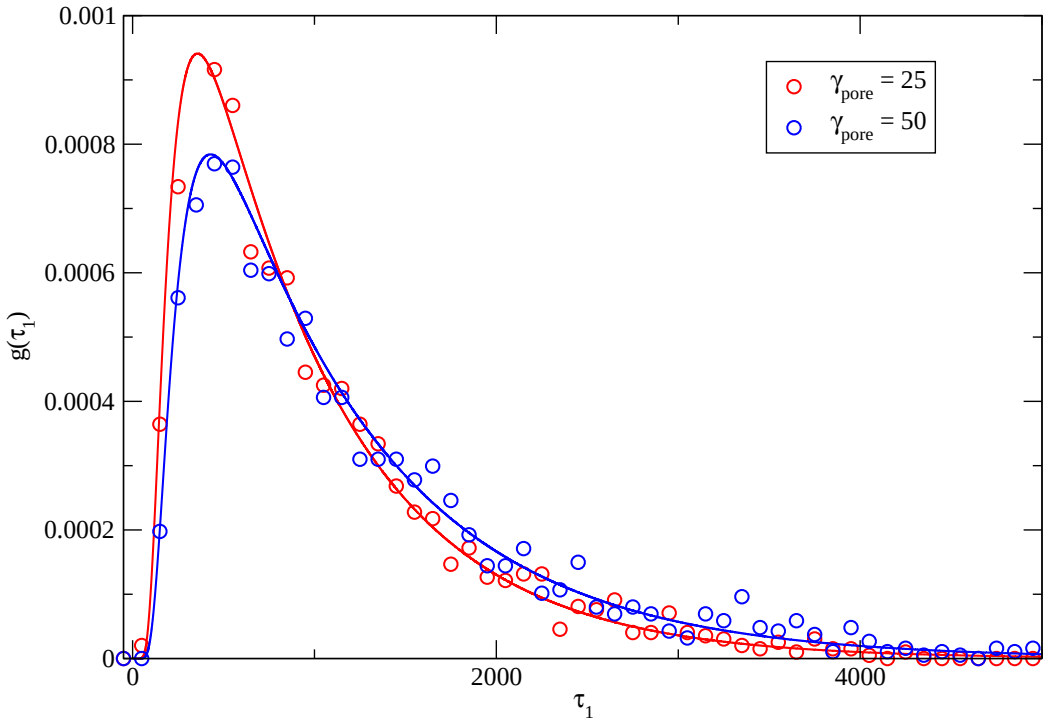

Figure 5.9: Unbiased translocation time distributions for a polymer of length $N = 31$ and $\gamma_{\text{pore}} = 25$ and 50, plotted on a linear scale. The open circles represent DPD simulation data and the solid curves shown FP theoretical predictions.

To illustrate the effect of the pore friction, the two previous figures were plotted together in Figure 5.9. The distribution for the higher pore friction parameter

stretches to higher translocation times, as expected. The calculated theoretical curves were parameterized by the overall friction coefficient of the entire polymer γ_{pol}, but effectively by the friction experienced by the monomers inside the pore. The curves for $\gamma_{\text{pore}} = 25$ and 50 were fit using values of $\gamma_{\text{pol}} = 25$ and 30, respectively. From Eq. (2.24), this would suggest values of $N_{\text{eff}} = 1$ and 3/5 for the number of monomers whose dynamics are affected by pore friction. These values were expected to be closer to the average number of monomers in the pore during translocation, $N_p \approx 3$. The discrepancy may be explained by the fact that only the middle layer (out of 3 total) of the pore particles influence the pore friction. Certainly extending this effect to the outer layers would increase N_{eff} but would also result in the pore friction affecting monomers outside the pore. Additionally, the complicated nature of the dissipative force in the DPD method, as shown in Eq. (3.3), could mean the relationship between γ_{pol} and γ_{pore} is not as simple as first thought. This is in contrast to a recent Brownian dynamics study in which a value for N_{eff} close to the approximated value was found in the case of sufficiently strong pore friction [32].

In this section, we have identified the regime in which pore friction is sufficiently high such that the polymer maintains quasi-equilibrium during unbiased translocation. We've also again demonstrated the presence of hydrodynamics in the scaling of translocation time with polymer length for low pore friction and good solvent conditions.

5.2.2 Biased

To drive translocation towards the *trans* reservoir, solvent quality on the *cis* side was made worse while that on the *trans* side remained the same. To quantify the variation, we define $\Delta a = a_{\text{cis}} - a_{\text{trans}}$ as the difference in the monomer-solvent interaction strength a_{ms} between the two reservoirs. This effect of solvent asymmetry is illustrated by the free energy profiles in Figure 5.10. The black curve at the top is a reference system to help distinguish between unbiased and biased translocation. Increasing the asymmetry parameter results in a marked decline of the free energy barrier height as Q increases. Evidently, it is energetically favourable for the polymer to be on the *trans* side relative to the *cis* side. This effect manifests as a sort of entropic driving force causing translocation to be biased towards the better quality solvent.

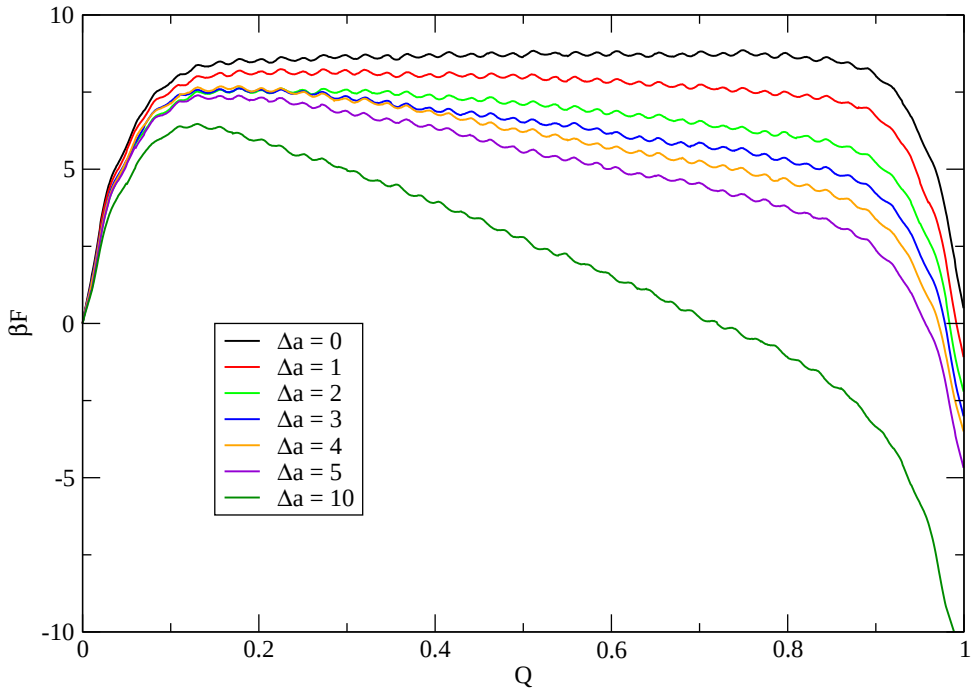

Figure 5.10: Free energy functions for a polymer of length $N = 21$ for different values of the solvent asymmetry parameter.

We next ran DPD simulations for the same set parameters and various polymer lengths. Figure 5.11 shows how translocation time scales with effective polymer length. As the asymmetric effect becomes more pronounced, the scaling exponent appears to asymptotically approach $\alpha = 1.11$, a value comparable to a previous HD prediction of $\alpha = 3\nu/(1+\nu) \approx 1.125$ for good solvent conditions and a constant driving force [34, 60]. Once again, this supports the validity of our DPD model in correctly incorporating hydrodynamic interactions. A prediction of the Fokker-Planck formalism is that the scaling exponent approaches $\alpha = 1$ in the case of a sufficiently strong driving force and pore friction [14, 62]. These conditions are evidently not accounted for in the presented simulations, as out-of-equilibrium scaling of $\alpha > 1$ was obtained. From the free energy profiles in Figure 5.10, we conclude that the entropic driving force

dictated by the difference in solvent quality is quite weak. A strong driving force would correspond to a free energy dominated by the chemical potential difference across the pore, and where the entropic barrier contribution is negligible [14]. Additionally, these simulations were run for a low value of pore friction ($\gamma_{\text{pore}} = \gamma = 4.5$). Since we wish to test the predictions of the FP formalism in the case of biased translocation, future simulations should involve both stronger pore friction and greater solvent asymmetry driving translocation.

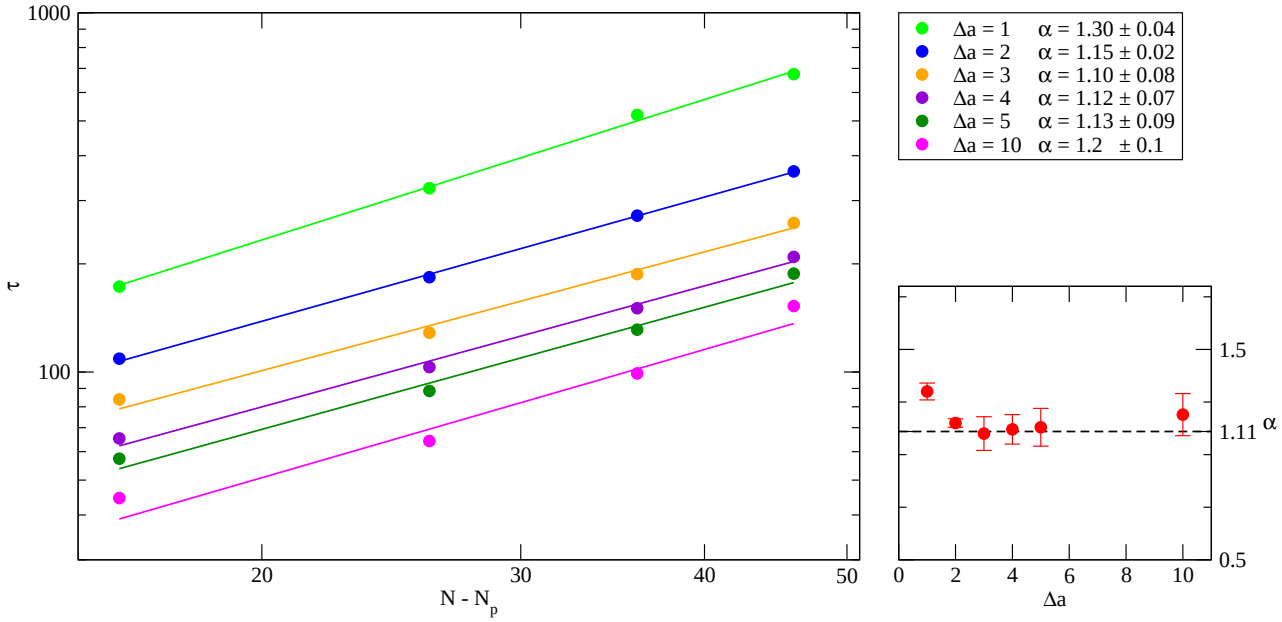

Figure 5.11: Mean translocation time vs. effective polymer length for various values of the solvent asymmetry parameter, fit to the power law $\tau \sim (N - N_p)^{\alpha}$. The subfigure shows the corresponding scaling exponents vs. difference in solvent quality. The dotted line indicates a theoretical prediction for α found for driven translocation in good solvent conditions and in the presence of HD interactions.

Although the quasi-equilibrium condition was not actualized in this section, we have verified that biased translocation between a good and poor solvent reservoir

yields preferential translocation towards the good solvent. The scaling exponent extracted from this process was found to agree with a theoretical prediction accounting for hydrodynamics, reinforcing our confidence that our DPD model is correctly exhibiting HD interactions.

Chapter 6

Conclusions and Future Work

In this thesis, we have utilized the dissipative particle dynamics and the Metropolis Monte Carlo simulation methods to investigate polymer behaviour and translocation dynamics in the presence of hydrodynamics.

We first examined a simple free polymer system to characterize the solvent quality effect in relation to our model, as well as confirm the existence of HD interactions. Scaling of the radius of gyration and chain relaxation time with polymer length yielded expected scaling exponents for good solvent conditions and hydrodynamics. For poor solvent conditions, the size exponent dropped as expected, but below the typical value of $\nu = 1/3$. This may be a consequence of the coarse-grained nature of the DPD method. Future work could investigate the asymptotic limit of ν for worse solvent quality to elucidate the anomaly.

To test predictions of the Fokker-Planck formalism, we next studied unbiased translocation while varying pore friction. A regime in which pore friction dominates the translocation was identified, and translocation distributions were found to agree

with the FP predictions. Also, for good solvent conditions and low pore friction, translocation time scaling was found to agree with a proposed theory for the Zimm model ($\alpha = 1 + 2\nu$). Further work needs to be done to identify the quasi-equilibrium regime. Time constraints and lack of computational resources meant translocation time distributions for only intermediate values of the pore friction could be compared to theory. More simulations of high pore friction should be run to confirm that the asymptotic limit $\alpha = 2$ is being reached. Additionally, it is currently unknown how the polymer friction parameter γ_{pol} used in the FP formalism relates to the DPD model. A relationship here is more opaque than other models due to the complicated nature of the dissipative force.

Lastly, translocation driven by asymmetric solvent quality was investigated. We found that the power law scaling of translocation time with polymer length agreed with a theoretical prediction incorporating hydrodynamics ($\alpha = 3\nu/(1 + \nu)$), but the quasi-equilibrium regime has not yet been identified. Greater asymmetries in solvent quality (higher entropic driving force) and greater pore friction would be the next steps in approaching the FP predicted $\alpha = 1$. Furthermore, a perhaps better way to test for quasi-equilibrium would be to examine the conformational behaviour of the subchains. This was attempted in our study, but poor statistics resulted in inconclusive data.

Above all else, future work should involve longer polymer chains, as the data presented here was from simulations of lengths no higher than $N = 51$. Other parameters such as pore length, radius and geometry (e.g. conical) could also be varied to examine their effect on translocation.

Bibliography

[1] D. Klemm, B. Heublin, H. P. Fink, and A. Bohn, Angew, Chem. Int. Ed. **44**, 3358 (2005).

[2] N. Campbell and J. Reece, *Biology* (Pearson Bejamin Cummings, San Francisco, CA, 2008), 8th ed.

[3] S. Brocchini, Adv. Drug Deliv. Rev. **53**, 123 (2001).

[4] D. R. Paul and L. M. Robeson, Polymer **49**, 3187 (2008).

[5] H. Shirakawa, E. J. Louis, and A. G. MacDiarmind, J. Chem. Soc., Chem. Commun. **16**, 578 (1977).

[6] M. Rubinstein and R. Colby, *Polymer Physics* (Oxford University Press, New York, 2003).

[7] P. E. Rouse, J. Chem. Phys. **21**, 1272 (1953).

[8] B. H. Zimm, J. Chem. Phys. **24**, 269 (1956).

[9] M. J. Khoury, W. Burke, and E. J. Thomson, Am. J. Hum. Gen. **69**, 1154 (2001).

[10] National Human Genome Research Institute, *DNA structure and bases*, `www.genome.gov/Pages/Hyperion//DIR/VIP/Glossary/Illustration/Images/dna.gif` (2006), online; accessed 2013-11-05.

[11] F. Sanger, S. Nicklen, and R. Coulson, Proc. Natl. Acad. Sci. **74**, 5463 (1977).

[12] D. R. Bentley, Curr. Opin. Genet. Dev. **16**, 545 (2006).

[13] L. T. C. França, E. Carrilho, and T. B. L. Kist, Q. Rev. Biophys. **35**, 169 (2002).

[14] M. Muthukumar, *Polymer Translocation* (CRC Press, Boca Raton, FL, 2011).

[15] B. Alberts, A. Johnson, J. Lewis, M. Raff, K. Roberts, and P. Walter, *Molecular Biology of the Cell* (Garland Science, New York, NY, 2007).

[16] J. Kasianowicz, E. Brandin, D. Branton, and D. Deamer, Proc. Natl. Acad. Sci. USA **93**, 13770 (1996).

[17] J. J. Nakane, M. Akeson, and A. Marziali, J. Phys.: Condens. Matter **15**, R1365 (2003).

[18] A. Meller, L. Nivon, E. Brandin, J. Golovchenko, and D. Branton, Proc. Natl. Acad. Sci. USA **97**, 1079 (2000).

[19] M. Muthukumar, Annu. Rev. Biophys. Biomol. Struct. **36**, 435 (2007).

[20] H. Chang, F. Kosari, G. Andreadakis, M. A. Alam, G. Vasmatzis, and R. Bashir, Nano Lett. **4**, 1551 (2004).

[21] S. M. Iqbal, D. Akin, and R. Bashir, Nature Nanotechnol. **2**, 243 (2007).

[22] A. J. Storm, J. H. Chen, H. W. Zandbergen, and C. Dekker, Phys. Rev. E **71**, 051903 (2005).

[23] D. Fologea, M. Gershow, B. Ledden, D. S. McNabb, J. A. Golovchenko, and J. Li, Nano Lett. **5**, 1905 (2005).

[24] S. W. Kowalczyk, A. R. Hall, and C. Dekker, Nano Lett. **10**, 324 (2010).

[25] M. Wanunu, J. Sutin, B. McNally, A. Chow, and A. Meller, Biophys. J. **95**, 4716 (2008).

[26] Oxford Nanopore Technologies, *Nanopore sensing*, `https://www.nanoporetech.com/technology/introduction-to-nanopore-sensing`, online; accessed 2013-10-20.

[27] D. Branton, D. W. Deamer, A. Marziali, H. Bayley, S. A. Benner, et al., Nat. Biotechnol. **26**, 1146 (2008).

[28] C. M. Edmonds, Y. C. Hudiono, A. G. Ahmadi, P. J. Hesketh, and S. Nair, J. Chem. Phys. **136**, 065105 (2012).

[29] D. Frenkel and B. Smit, *Understanding Molecular Simulation: From Algorithms to Applications* (Academic Press, San Diego, 2001).

[30] F. Müller-Plathe, ChemPhysChem **3**, 755 (2002).

[31] I. Huopaniemi, K. Luo, T. Ala-Nissila, and S.-C. Ying, J. Chem. Phys. **125**, 124901 (2006).

[32] J. M. Polson and T. Dunn (2014), arXiv preprint arXiv:1401.8253.

[33] S. Matysiak, A. Montesi, M. Pasquali, A. B. Kolomeisky, and C. Clementi, Phys. Rev. Lett. **96**, 118103 (2006).

[34] F. Kapahnke, U. Schmidt, D. W. Heermann, and M. Weiss, J. Chem. Phys. **132**, 164904 (2010).

[35] H. W. de Haan and G. W. Slater, J. Chem. Phys. **136**, 204902 (2012).

[36] H. C. Loebl, R. Randel, S. P. Goodwin, and C. C. Matthai, Phys. Rev. Lett. **96**, 118103 (2006).

[37] T. Ikonen, A. Bhattacharya, T. Ala-Nissilia, and W. Sung, Phys. Rev. E. **85**, 051803 (2012).

[38] A. Milchev, J. Phys.: Condens. Matter **23**, 103101 (2011).

[39] C. Pierleoni and C.-P. Ryckaert, Phys. Rev. Lett. **66**, 2992 (1991).

[40] J. M. Polson and J. P. Gallant, J. Chem. Phys. **124**, 184905 (2006).

[41] V. V. Lehtola, R. P. Linna, and K. Kaski, Phys. Rev. E **81**, 031803 (1991).

[42] M. K. Petersen, J. B. Lechman, S. J. Plimpton, G. S. Grest, and P. R. Schunk, J. Chem. Phys. **132**, 174106 (2010).

[43] J. P. Hernandez-Ortiz, M. Chopra, S. Geier, and J. J. de Pablo, J. Chem. Phys. **131**, 044904 (2009).

[44] P. Ahlrichs and Dünweg, J. Chem. Phys. **111**, 8225 (1999).

[45] Y. Kong, C. W. Manke, W. G. Madden, and A. G. Schlijiper, J. Chem. Phys. **107**, 592 (1997).

[46] W. Jiang, J. Huang, and M. Laradji, J. Chem. Phys. **126**, 044901 (2007).

[47] X. Li, I. G. Pivkin, and H. Liang, Polymer **54**, 4309 (2013).

[48] K. Yang, A. Vishnyakov, and A. V. Neimark, J. Phys. Chem. B **117**, 3648 (2013).

[49] M. G. Hughes, *Dissipative particle dynamics simulations of polymers in the presence of hydrodynamics*, University of Prince Edward Island (2013), honours thesis.

[50] W. Sung and P. J. Park, Phys. Rev. Lett. **77**, 783 (1996).

[51] M. Muthukumar, J. Chem. Phys. **111**, 10371 (1999).

[52] J. Chuang, Y. Kantor, and M. Kardar, Phys. Rev. E **65**, 011802 (2001).

[53] K. Luo, T. Ala-Nissila, and S.-C. Ying, J. Chem. Phys. **124**, 034714 (2006).

[54] D. Wei, W. Yang, X. Jin, and Q. Liao, J. Chem. Phys. **126**, 204901 (2007).

[55] K. Luo, T. T. Ollila, I. Huopaniemi, T. Ala-Nissila, P. Pomorski, S.-C. Ying, and A. Bhattacharya, Phys. Rev. E **78**, 050901 (2008).

[56] F. Mondaini and L. Moriconi, Phys. Lett. A. **276**, 2903 (2012).

[57] D. Panja, G. T. Barkema, and R. C. Ball, J. Phys.: Condens. Matter **19**, 432202 (2007).

[58] M. G. Gauthier and G. W. Slater, J. Chem. Phys. **128**, 205103 (2008).

[59] C. M. Edmonds, P. J. Hesketh, and S. Nair, J. Chem. Phys. **425**, 1 (2013).

[60] H. Vocks, D. Panja, G. Barkema, and R. Ball, J. Phys.: Condens. Matter **20**, 095224 (2008).

[61] S. Melchionna, M. Bernaschi, M. Fyta, E. Kaxiras, and S. Succi, Phys. Rev. E. **79**, 030901R (2009).

[62] T. Ikonen, A. Bhattacharya, T. Ala-Nissilia, and W. Sung, Europhys. Lett. **103**, 38001 (2013).

[63] J. M. Polson and A. C. M. McCaffrey, J. Chem. Phys. **138**, 174902 (2013).

[64] H. W. de Haan and G. W. Slater, J. Chem. Phys. **134**, 154905 (2011).

[65] P.-G. de Gennes, *Scaling Concepts in Polymer Physics* (Cornell University Press, London, 1979).

[66] E. Eisenriegler, K. Kremer, and K. Binder, J. Chem. Phys. **77**, 6296 (1982).

[67] A. Vishnyakov, D. S. Talaga, and A. V. Neimark, Phys. Chem. Lett. **3**, 3081 (2012).

[68] N. Goga, A. J. Rzepiela, A. H. Vries, S. J. Marrink, and H. J. C. Berendsen, J. Chem. Theory Comput. **3**, 3081 (2012).

[69] M. Langeloth, M. Yuichi, M. C. Böhm, and F. Müller-Plathe, J. Chem. Phys. **138**, 104907 (2013).

[70] P. J. Hoogerbrugge and J. M. V. A. Koelman, Europhys. Lett. **19**, 115 (1992).

[71] P. Español and P. Warren, Europhys. Lett. **30**, 191 (1995).

[72] R. D. Groot and P. B. Warren, J. Chem. Phys. **107**, 4423 (1997).

[73] O. K. Rice, J. Chem. Phys. **12**, 1 (1944).

[74] F. Mallamace and H. E. Stanley, *Complex Materials in Physics and Biology* (IOS Press, Amsterdam, 2012).

[75] D. C. Visser, H. C. J. Hoefsloot, and P. D. Iedema, J. Comput. Phys. **207**, 626 (2005).

[76] A. W. Lees and S. F. Edwards, J. Phys. C: Solid State Phys. **5**, 1921 (1972).

[77] M. Revenga, I. Zuniga, and P. Español, Comput. Phys. Commun. **121-122**, 309 (1999).

[78] I. V. Pivkin and G. E. Karniadakis, J. Comput. Phys. **207**, 114 (2005).

[79] R. B. Groot and P. B. Warren, J. Chem. Phys. **107**, 4423 (2001).

[80] J. Feng, X. Ge, L. Zhou, H. Lio, and Y. Hu, Fluid Phase Equilib. **302**, 26 (2011).

[81] J. Guo, X. Li, and H. Liang, J. Chem. Phys. **134**, 134906 (2011).

[82] N. A. Spenley, Europhys. Lett. **49**, 534 (1999).

[83] J. M. Ilnytskyi and Y. Holovatch, Condens. Matt. Phys. **10**, 539 (2007).

[84] J. M. Polson, M. Fatehi Hassanabad, and A. C. M. McCaffrey, J. Chem. Phys. **138**, 024906 (2013).